HAL
open science

# A new velocity field for Africa from combined GPS and DORIS space geodetic Solutions: Contribution to the definition of the African reference frame (AFREF)

E. Saria, E. Calais, Z. Altamimi, P. Willis, H. Farah

▶ **To cite this version:**

E. Saria, E. Calais, Z. Altamimi, P. Willis, H. Farah. A new velocity field for Africa from combined GPS and DORIS space geodetic Solutions: Contribution to the definition of the African reference frame (AFREF). Journal of Geophysical Research : Solid Earth, 2013, 118, pp.1677-1697. 10.1002/jgrb.50137 . insu-03581797

**HAL Id: insu-03581797**

**https://insu.hal.science/insu-03581797v1**

Submitted on 20 Feb 2022

**HAL** is a multi-disciplinary open access archive for the deposit and dissemination of scientific research documents, whether they are published or not. The documents may come from teaching and research institutions in France or abroad, or from public or private research centers.

L'archive ouverte pluridisciplinaire **HAL**, est destinée au dépôt et à la diffusion de documents scientifiques de niveau recherche, publiés ou non, émanant des établissements d'enseignement et de recherche français ou étrangers, des laboratoires publics ou privés.

Copyright

# A new velocity field for Africa from combined GPS and DORIS space geodetic Solutions: Contribution to the definition of the African reference frame (AFREF)

E. Saria,[1,6] E. Calais,[2] Z. Altamimi,[3] P. Willis,[4,7] and H. Farah[5]

Received 17 September 2012; revised 31 January 2013; accepted 15 February 2013; published 8 April 2013.

[1] We analyzed 16 years of GPS and 17 years of Doppler orbitography and radiopositioning integrated by satellite (DORIS) data at continuously operating geodetic sites in Africa and surroundings to describe the present-day kinematics of the Nubian and Somalian plates and constrain relative motions across the East African Rift. The resulting velocity field describes horizontal and vertical motion at 133 GPS sites and 9 DORIS sites. Horizontal velocities at sites located on stable Nubia fit a single plate model with a weighted root mean square residual of 0.6 mm/yr (maximum residual 1 mm/yr), an upper bound for plate-wide motions and for regional-scale deformation in the seismically active southern Africa and Cameroon volcanic line. We confirm significant southward motion (∼1.5 mm/yr) in Morocco with respect to Nubia, consistent with earlier findings. We propose an updated angular velocity for the divergence between Nubia and Somalia, which provides the kinematic boundary conditions to rifting in East Africa. We update a plate motion model for the East African Rift and revise the counterclockwise rotation of the Victoria plate and clockwise rotation of the Rovuma plate with respect to Nubia. Vertical velocities range from –2 to +2 mm/yr, close to their uncertainties, with no clear geographic pattern. This study provides the first continent-wide position/velocity solution for Africa, expressed in International Terrestrial Reference Frame (ITRF2008), a contribution to the upcoming African Reference Frame (AFREF). Except for a few regions, the African continent remains largely under-sampled by continuous space geodetic data. Efforts are needed to augment the geodetic infrastructure and openly share existing data sets so that the objectives of AFREF can be fully reached.

**Citation:** Saria, E., E. Calais, Z. Altamimi, P. Willis, and H. Farah (2013), A new velocity field for Africa from combined GPS and DORIS space geodetic solutions: Contribution to the definition of the African reference frame (AFREF), *J. Geophys. Res. Solid Earth*, *118*, 1677–1697, doi:10.1002/jgrb.50137.

## 1. Introduction

[2] Space geodesy, in particular the Global Positioning System (GPS), is now routinely used to determine continent-wide positions and velocity fields in a well-defined reference frame for both surveying and geophysical applications [*Altamimi et al.*, 2011]. Initiatives such as European Reference Frame in Europe [*Bruyninx et al.*, 2012] or its equivalent North American Reference Frame in North America [*Craymer and Piraszewski*, 2001] and Geocentric Reference System for the Americas in South America [*Sanchez et al.*, 2012] are examples where dense GPS measurements serve both the definition of a geodetic reference frame and the estimation of plate motion and crustal deformation [e.g., *Nocquet and Calais*, 2003; *Calais et al.*, 2006a]. The African continent, in spite of its large extent and its on-land plate boundaries in northern and eastern Africa (Figure 1), however lags behind, in part because of a paucity of quality geodetic observations. As a result, a proper continent-wide geodetic reference frame for Africa still does not exist, and our understanding of the kinematics of its major plate boundaries remains limited.

[3] Initiatives to improve the geodetic infrastructure in Africa are however underway. Individual countries are now investing in continuously observing geodetic networks for

Additional supporting information may be found in the online version of this article.

[1]Ardhi University, School of Geospatial Sciences and Technology, Dar es Salaam, Tanzania.
[2]Ecole Normale Supérieure, Department of Geosciences, Paris, France.
[3]Institut National de l'Information Géographique et Forestière (IGN), LAREG, Marne-la-Vallée, France.
[4]Institut National de l'Information Géographique et Forestière (IGN), Direction Technique, Saint Mandé, France.
[5]Regional Center for Mapping of Resources for Development (RCMRD), Nairobi, Kenya.
[6]Also at Department of Earth, Atmospheric and Planetary Sciences, Purdue University, West Lafayette, Indiana, USA.
[7]Univ Paris Diderot, Sorbonne Paris Cité, Institut de Physique du Globe de Paris, Paris, France.

Corresponding author: E. Saria, Department of Earth, Atmospheric and Planetary Sciences, Purdue University 550 Stadium Mall Drive, West Lafayette, IN 47907, USA. (esaria@purdue.edu)

©2013. American Geophysical Union. All Rights Reserved.
2169-9313/13/10.1002/jgrb.50137

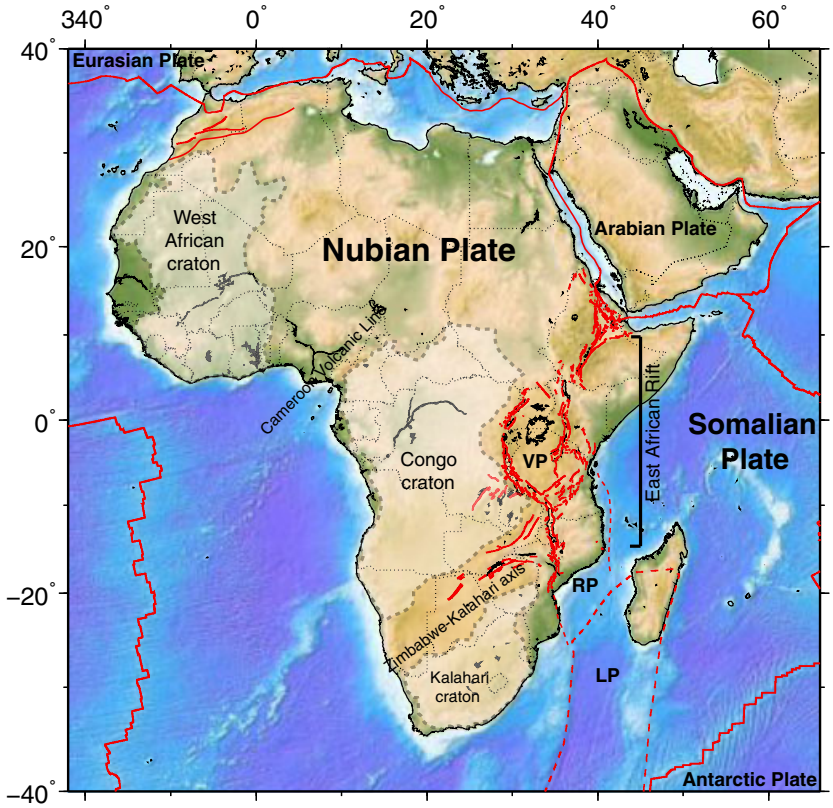


**Figure 1.** Tectonic context of Africa, outlining the major tectonic features discussed in the text. Grey dashed lines show the main cratons. Red lines show the major plate boundaries, solid where they are well defined, dashed where they are assumed. VP: Victoria Plate, RP: Rovuma Plate, LP: Lwandle Plate.

surveying and deformation monitoring applications. These efforts are led by the United Nation Economic Commission for Africa and are coordinated at multinational scale by International Association of Geodesy as a member of the Steering Committee through its subcommission on "African Reference Frame" (AFREF). These efforts aim at augmenting the geodetic infrastructure in Africa and at defining a common three-dimensional reference frame for the whole continent tied to the International Terrestrial Reference Frame (ITRF) [*Altamimi et al.*, 2011]. Africa indeed includes 57 countries of which 53 have their own coordinate system [*Wonnacott*, 2005, 2006], with significant variations among countries regarding the state of these systems and the extent of their usage. This causes issues for intercountry mapping, in particular when access to natural resources is involved. In order to provide this unified reference frame, AFREF will need an accurate definition of stable Nubia consistent with the precision level of intraplate GPS measurements, and an accurate kinematic model for its actively deforming regions such as north and east Africa.

[4] Research initiatives from investigators interested in the geodynamics of Africa's plate boundaries or in its climatic evolution are also participating in increasing the number of GPS stations in portions of the continent [e.g., *Cilliers et al.*, 2003; *Bock et al.*, 2008; *Nahmani et al.*, 2012]. Finally, the AfricaArray international project is adding a geodetic component to its primarily seismological efforts with 20 new stations across the continent (www.africaarray.psu.edu). The number of continuously operating GPS stations (cGPS) in Africa is therefore expanding rapidly. As a consequence, it is now possible to significantly improve upon previous studies of Nubia/Somalia kinematics, or deformation and plate motions with the East African Rift [*Nocquet et al.*, 2006; *Calais et al.*, 2006b; *Stamps et al.*, 2008], as well as more generally contribute to AFREF's goal of a unified reference frame for Africa.

[5] Here we present an analysis of up to 16 years of GPS data at 133 sites and up to 17 years of Doppler Orbitography and Radiopositioning Integrated by Satellite (DORIS) data at nine sites (Figure 2) to produce a new position/velocity solution for Africa. We compare data processing strategies and pay particular attention to the estimation of velocity uncertainties. We use the resulting velocities to assess the level of rigidity of stable Nubia and estimate the angular rotation vectors that describe the motion of stable Nubia and its neighboring plates, in particular across the East African Rift.

## 2. Tectonic Context of Africa

[6] Africa is characterized by contrasted long wavelength topography, with a series of basins and swells superimposed on a large-scale bimodal elevation distribution, with high plateaus in the southern and eastern parts of the continent (∼1000 to 2000 m) and lower elevations in its central and western parts [*Holmes*, 1945; *Doucouré and De Wit*, 2003]. High elevation southern and eastern Africa is usually thought to result from the dynamic support of the

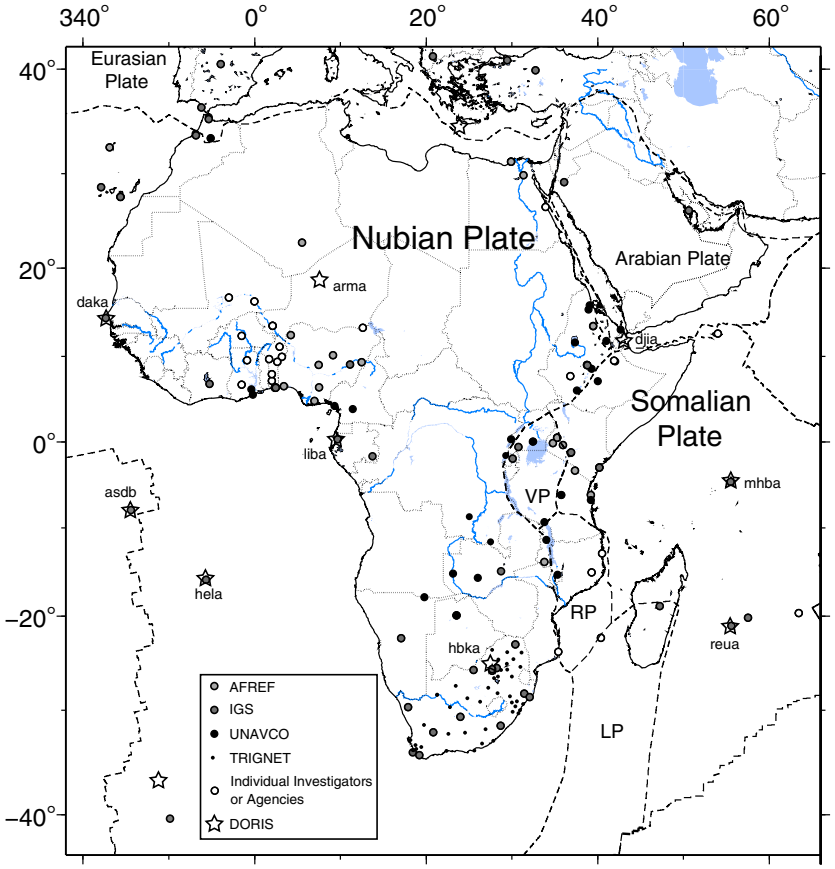


**Figure 2.** Distribution of the continuous GPS and DORIS sites used in this study. Sites are color-coded as a function of their availability. AFREF = African Reference Frame database; IGS = International Global Navigation Satellite Systems (GNSS) Service data centers; UNAVCO = University NAVSTAR Consortium (UNAVCO) archive; TRIGNET = South Africa Mapping Agency archive. Sites labeled "individual investigators or agencies" are generally not available online. Many other continuous GPS sites operate in Africa whose data are not made public. VP: Victoria Plate, RP: Rovuma Plate, LP: Lwandle Plate.

buoyant "African superplume" [*Lithgow-Bertelloni and Silveri*, 1998], a large low-velocity seismic anomaly rooted at the core-mantle boundary and rising through the mantle to reach the uppermost mantle under eastern Africa [*Ritsema et al.*, 1999; *Behn et al.*, 2004]. *Quéré and Forte* [2006] argue that coupling between the African superplume and the lithosphere drove the opening of the East African Rift. However, the present day uplift caused by this deep, buoyant, mantle anomaly may not exceed 0.12 mm/yr [*Gurnis et al.*, 2000; *Moucha and Forte*, 2011]. The correlation between slow seismic velocity anomalies in the upper mantle and long wavelength positive gravity anomalies is nevertheless indicative that the current large-scale topography of Africa is convectively supported [*Al-Hajri et al.*, 2009]. Flexural support appears unlikely for most of Africa, as shown by the fact that most domal regions are correlated with thin plate thickness [*Pérez-Gussinyé et al.*, 2009].

[7] The core of the African continent consists of three main Archean cratons (West African, Congo, Kalahari) and smaller cratonic fragments that were juxtaposed during the assembly of Pangea about 3.6 billion years ago [*Begg et al.*, 2009, Figure 1]. These cratons are thought to have remained undisturbed tectonically since the Archean, except for minor reheating attested by Tertiary kimberlites [e.g., *Chesley et al.*, 1999]. They are separated from each other by weaker, and sometimes still seismically active, orogenic belts [*Tokam*, 2010; *Begg et al.*, 2009]. Seismic, xenolith, and gravity data show that the cratons are colder and stronger than these surrounding orogenic belts and are underlain by 200 to 300 km thick lithospheric keels [*Nyblade et al.*, 2000; *Weeraratne et al.*, 2003].

[8] The Cameroon volcanic line, which forms the boundary between the West African and Congo cratons, is among these weak zones (Figure 1). It is characterized by moderate magnitude earthquakes and active volcanism [*Tokam*, 2010; *Moreau et al.*, 1987; *Vicat et al.*, 2002]. Similarly, active seismic belts coincident with Panafrican orogenic belts separate the cratons of southern Africa, with present-day topographic features suggestive of incipient continental breakup in the middle of the Nubian plate [*Sebagenzi and Kaputo*, 2002]. A series of NE-trending active grabens west of the Tanganyika-Malawi segment of the East African Rift that extends into the Democratic Republic of Congo [*Delvaux and Barth*, 2009] is associated with recent uplift along the Zimbabwe-Kalahari axis [*Kinabo et al.*, 2007]. Evidence for belts of seismic activity and geomorphic structures indicative of active tectonics in the interior of the Nubian plate raise questions as to the rigidity level of the

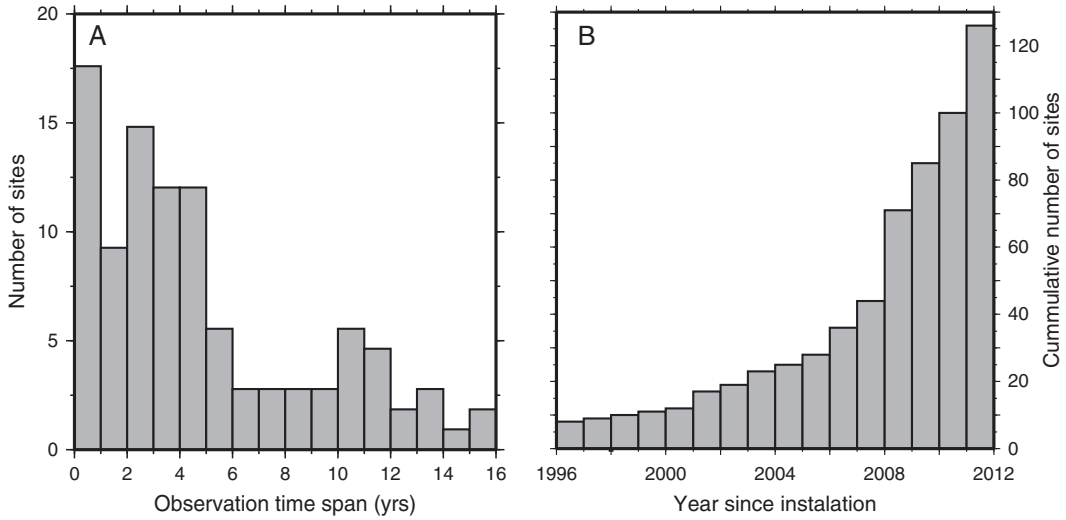


**Figure 3.** (A) Number of continuous GPS sites in Africa used in this study as a function of observation time span. Many sites are still "young," with less than 5 years of continuous observations. (B) Histogram showing the cumulative number of continuous GPS sites in Africa from 1996 to 2012. Note the rapid increase since 2008.

African continent and whether we are currently witnessing incipient breakup in part of it.

[9] Superimposed on these features are two major active plate boundaries. In northern Africa, Nubia and Eurasia are converging obliquely at 2 to 6 mm/yr [*Nocquet and Calais*, 2003; *McClusky et al.*, 2003]. This motion is taken up by recent strike-slip and shortening in a narrow coastal band along most of northern Africa [*Meghraoui et al.*, 1986; *Gomez et al.*, 2000; *Mahsas et al.*, 2008]. In addition, recent GPS measurements in Morocco show southward motions with respect to Nubia that are best explained by the delamination and southward rollback of the African lithospheric mantle [*Fadil et al.*, 2006].

[10] Finally, the East African Rift (EAR), a 5000 km long series of fault-bounded depressions straddling East Africa in a roughly NS direction, marks the divergent boundary between the Nubian and Somalian plates in eastern Africa. Seismicity, active faulting, and volcanism in the EAR are generally localized along narrow belts separating largely aseismic domains (Figure 1). This led *Hartnady* [2002] to postulate that the EAR consisted of a mosaic of tectonic blocks separated by active grabens and transfer zones. *Calais et al.* [2006b], then *Stamps et al.* [2008] showed that geodetic data, earthquake slip vectors, and 3.2 Myr average oceanic spreading rates and transform-fault azimuths (from *Horner-Johnson et al.* [2007]) were consistent with a kinematic model that includes three subplates (Victoria, Rovuma, and Lwandle) imbedded in the plate boundary zone between Nubia and Somalia. However, their model relied on very few GPS sites—none on Rovuma and Lwandle—and was hence quite uncertain for these plates. Their estimates of the Nubia-Somalia angular velocity are overall consistent with other geodetic estimates [*Sella et al.*, 2002; *Prawirodirdjo and Bock*, 2004; *Nocquet et al.*, 2006] and a recent estimate based on 3.2 Myr average oceanic data only [*Horner-Johnson et al.*, 2007]. The significant scatter between these various estimates reflects sparse space geodetic data covering the Nubian and (mostly) Somalian plates as well as differences in reference frame implementation through time.

[11] Increased spatial coverage from space geodetic techniques, improved processing strategies, and a well-defined reference frame are essential to assess the level of internal deformation of the Nubian plate and to quantify plate boundary deformation at its northern and eastern boundaries. An accurate and precise assessment of these parameters, in three dimensions, is essential to the definition and maintenance of a reference frame for Africa, given that the precision of precise surveying measurements now reaches the centimeter level.

## 3. Input Data

### 3.1. GPS Data and Processing

[12] The GPS data set processed here includes 16 years of observations (1996 to 2011) at all cGPS sites where data is openly shared. This represents 29 cGPS sites available at the International GNSS Service (IGS) [*Dow et al.*, 2009] and 104 additional cGPS sites operated by various independent geodetic groups (Figure 2). Many other cGPS stations are currently operating in Africa but their data is not made openly available at this point by network operators or some individual investigators. In addition to cGPS sites, we included data from 35 episodic GPS sites located in Tanzania with surveys spanning 2005–2011, whose data is available via the UNAVCO archive [www.unavco.org].

[13] Although we processed all openly available cGPS sites in Africa, we only use in this paper sites with a minimum of 2.5 years of continuous observations. This represents the minimum amount of time necessary to average out seasonal noise, unrelated to the long-term motions of interest here, and obtain a reliable velocity estimate [*Blewitt and Lavallée*, 2002]. Years 2010 and 2011 saw a rapid increase in cGPS site deployments in Africa

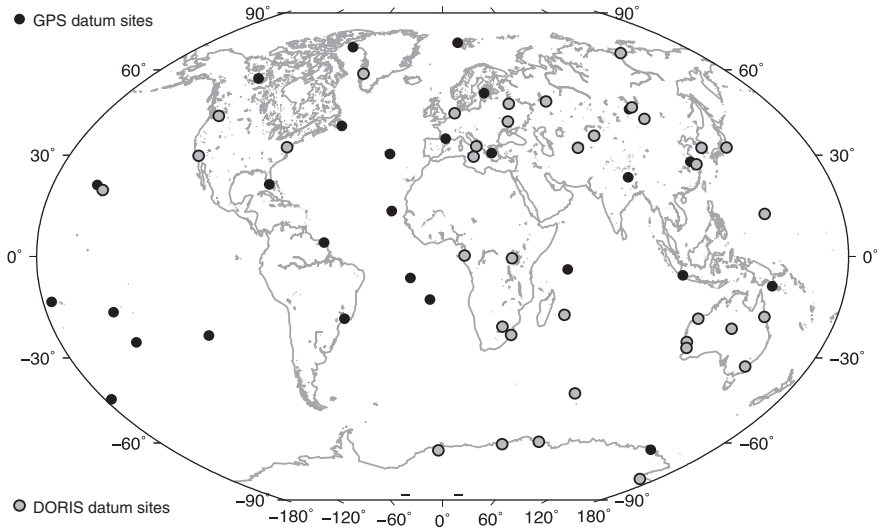


**Figure 4.** Distribution of GPS and DORIS global core sites used in the reference frame implementation (explanations in the text). Note the good spatial distribution of sites in the northern and southern hemispheres, with 17 and 15 DORIS sites, and 17 and 16 GPS sites, respectively.

(Figure 3). At the current deployment rate, the number of sites with reliable velocities will have increased by at least a factor of 2 in the next 2 years.

[14] We processed the GPS data using the GAMIT-GLOBK software package [*Herring et al.*, 2010] following a processing strategy described in detail in *Nocquet et al.* [2006]. GPS measurements analysis software was developed at Massachusetts Institute of Technology. We used double-differenced GPS phase measurements to estimate daily station coordinates, satellite state vectors, seven tropospheric delay parameters per site and per day, two horizontal tropospheric gradients per day, and phase ambiguities using IGS final orbits and Earth orientation parameters. We applied absolute antenna phase center models following the tables recommended by the IGS [*Schmid et al.*, 2007], solid Earth and polar tide corrections following the IERS standards [*McCarthy and Petit*, 2003], and ocean loading corrections using the FES2004 ocean tide model [*Lyard et al.*, 2006] with the eight principal diurnal and semidiurnal tidal constituents.

[15] The resulting least squares adjustment vector and its corresponding variance-covariance matrix for station positions and orbital elements estimated for each independent daily solution were then combined with global SINEX (Solution Independent Exchange format) files from the IGS daily processing routinely done at the Massachusetts Institute of Technology using GLOBK. This global combination allows us to optimally tie our solution to the latest ITRF thanks to a large number of globally distributed common sites, which strengthen the minimal constraint solution presented below. We then implemented the reference frame for each daily unconstrained global solution by minimizing the position deviations of 33 IGS core stations (Figure 4) with respect to ITRF2008 [*Altamimi et al.*, 2011] while estimating seven Helmert parameters (three for translation, three for rotation, and one for scale). In this process, because of the reduced precision of the vertical component in standard GPS solutions, we down-weighted the variance of the height coordinates by a factor of 10 compared to the horizontal components.

[16] We used these daily solutions to produce position time series, which we thoroughly examine to identify outliers, offsets, or discontinuities. We quantified and corrected for offsets by modeling site positions as the sum of (1) a linear term representing secular displacement, (2) an annual and semiannual periodic term representing seasonal effects not modeled in the GPS data analysis, and (3) discontinuities due to equipment changes or problems at the site. The model equation is, for each component (north, east, up), the following:

$$y = at + b + \sum_{i=1}^{N} c_i H_i(t) + d\sin(2\pi t) + e\cos(2\pi t) + f\sin(4\pi t) + g\cos(4\pi t) \quad (1)$$

where $a, b, c, d, e, f,$ and $g$ are estimated by inverting site positions $y$ at time $t$ (in years) using a singular value decomposition scheme. $H_i$ is a binary operator equal to zero or one before or after offset $i$, respectively. Most sites, even those with frequent offsets such as HRAO, PRE1, PRE2 (South Africa), KISM (Kenya), and WIND (Namibia), have been reliably corrected. However, sites ASMA (Eitrea) and ALX2 (Egypt) showed too many outliers (i.e., positions that differ from the long-term trend of the position time series by more than three sigmas) and offsets and had to be removed from the final solution.

[17] We assessed the quality of the resulting position time series by calculating the daily position scatter from the mean using the following weighted root mean square definition:

$$WRMS = \sqrt{\frac{N}{N-1} \frac{\sum_{i=1}^{N} \frac{(y_i-(a+bt_i))^2}{\sigma_i^2}}{\sum_{i=1}^{N} \sigma_i^2}} \quad (2)$$

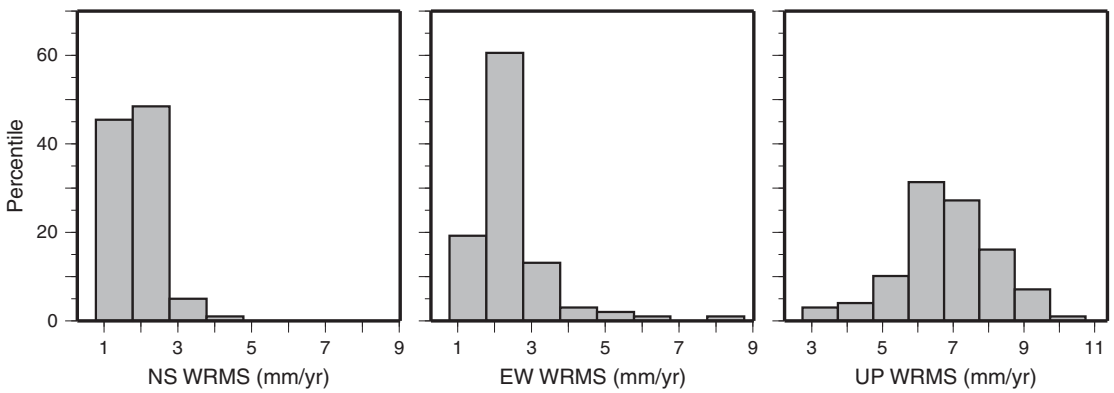


**Figure 5.** Precision of the GPS solution presented here as examined from the daily scatter (or long-term repeatability) of individual daily positions.

where $y_i$ and $\sigma_i$ are the site position and its associated formal error, $a$ and $b$ the parameters that define the best-fit straight line through the position time series, and $N$ is the total number of positions [*Larson and Agnew*, 1991]. We found WRMS of 1.5 mm on average (3 mm maximum) for the horizontal position components and 6 mm on average (10 mm maximum) for the vertical position component (Figure 5). This result is consistent with other continent-wide studies [e.g., *Nocquet et al.*, 2005; *Calais et al.*, 2006a].

[18] Once the daily solutions had been cleaned, we combined them into loosely constrained weekly solutions using GLOBK in order to further reduce some of the daily position scatter. Weekly solutions also have the advantage of reducing the processing time necessary to produce the final, cumulative, position-velocity solution spanning the entire 1996.0–2012.0 time interval. These loosely constrained weekly solutions later become inputs to the combination described below.

### 3.2. DORIS Data and Processing

[19] DORIS is one of the four space geodetic techniques participating in the realization of the ITRF, with currently seven analysis centers, six enabled satellites, and a stable network of 57 ground stations since 2009. There are 98% of them that are installed on stable concrete pillars [*Tavernier et al.*, 2002; *Willis et al.*, 2010a]. As a result of the steady improvements in network quality and data analysis, the precision of DORIS positions currently reaches 10 mm in 3-D [*Willis et al.*, 2012].

[20] We used 17 years of weekly solutions from the IGN Analysis Center (solution ignwd08 [*Willis et al.*, 2010b]) using the GPS Inferred Positioning System (GIPSY)-Orbit Analysis Simulation Software (OASIS) II software [*Webb and Zumberge*, 1995; *Willis et al.*, 2005a] and covering the time interval from January 1993 to September 2011. The solutions result from a complete reprocessing of the entire DORIS data set expressed in free-network for the International DORIS Service (IDS), including the use of the GMF Mapping Function [*Boehm et al.*, 2006], an improved treatment of daily solar radiation pressure [*Gobinddass et al.*, 2009a, 2009b] as well as atmospheric drag [*Gobinddass et al.*, 2010]. Tropospheric zenith delays were estimated at the beginning of most satellite passes, as discussed in *Bock et al.* [2010]. Horizontal tropospheric gradients were not estimated. Standard phase center corrections were applied for satellites and ground antennas (vertical offset but no phase center variation model), as provided in the DORIS data files. We applied solid Earth and pol-e tides as recommended by IERS standards [IERS, 2003] as well as ocean loading using the FES2004 model [*Lyard et al.*, 2006]. Discontinuities in DORIS time series due to geophysical effects (nearby earthquakes, volcanic subsidence) or to antenna instabilities were corrected when building the time series using a method similar to the one described above for GPS [*Willis and Ries*, 2005].

[21] Similar to the GPS data, the DORIS observables are first processed in daily batches and then combined into weekly loosely constrained solutions, which form the basis for the combination described below. This DORIS combination uses the GIPSY-OASIS software package, combining the full covariance of daily estimations [*Willis et al.*, 2005b].

### 3.3. Combination

[22] Our combination uses the two-step procedure of the ITRF construction [*Altamimi et al.*, 2002, 2011]. The first step consists of stacking the minimally constrained weekly GPS and DORIS solutions described above to estimate a cumulative solution for each technique separately. The second step consists of combining these cumulative GPS and DORIS solutions together with local geodetic ties at colocated sites to produce a single combined long-term (*i.e.*, position-velocity) solution. The combination model is implemented in the Combination and Analysis of Terrestrial Reference Frame (CATREF) software [*Altamimi et al.*, 2002, 2011]. It is computationally efficient and allows for a rigorous combination of DORIS and GPS solutions using the full variance-covariance information of both. Its end product is a single cumulative position-velocity solution in a well-defined reference frame with its full variance-covariance information.

[23] The CATREF combination model is used for both steps. The method poses that the position of a site at a given epoch relates to its position at the epoch of the combination through its estimated linear velocity and a 14-parameter (Helmert) similarity transformation (translation, rotation, and scale changes) between the combined and individual

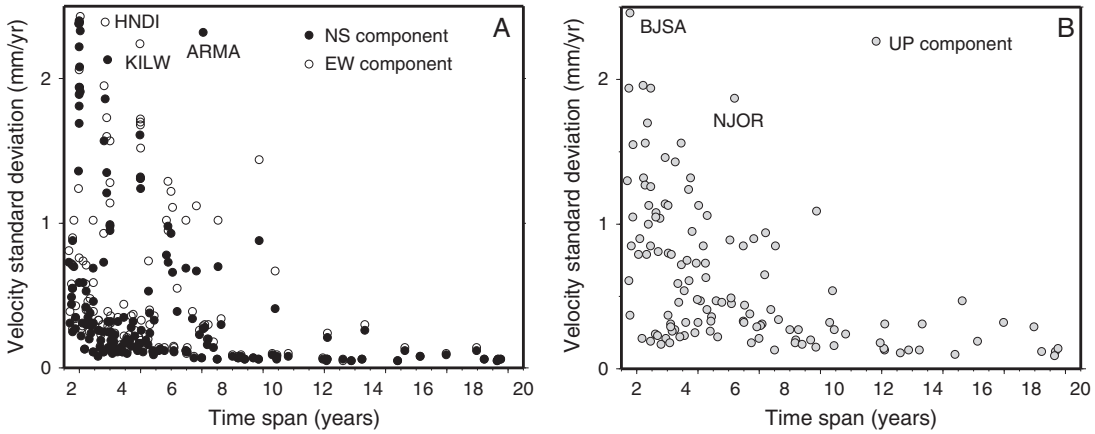


**Figure 6.** Velocity uncertainties from the CATREF combination as a function of observation time span (after applying a 1.5 scaling factor, see explanations in text). Uncertainties decrease rapidly during the first few years, then much slower after about 3 years of observation.

solutions, as described in the following equations [*Altamimi et al.*, 2011]:

$$X_s^i = X_{\text{comb}}^i + (t_s - t_0)\dot{X}_{\text{comb}}^i + T_k + D_k X_{\text{comb}}^i + R_k X_{\text{comb}}^i + (t_s - t_k)[\dot{T}_k + \dot{D}_k X_{\text{comb}}^i + \dot{R}_k X_{\text{comb}}^i] \quad (3)$$

$$\dot{X}_s^i = \dot{X}_{\text{comb}}^i + \dot{T}_k + \dot{D}_k X_{\text{comb}}^i + \dot{R}_k X_{\text{comb}}^i \quad (4)$$

where $X_s^i$ is the position of site $i$ in solution $s$, $X_{\text{comb}}^i$ and $\dot{X}_{\text{comb}}^i$ are the estimated position and its final velocity in the combination, respectively, and $T_k, D_k, R_k$ and $\dot{T}_k, \dot{D}_k, \dot{R}_k$ are the translation, scale, and rotation parameters and their time derivatives between individual solutions and the combined solution. $t_0$ is the reference epoch of the combined solution (typically the midpoint of the observation time span of the combined solution), $t_s$ is the epoch of the site coordinates in solution $s$, and $t_k$ is the reference epoch of the transformation parameters.

[24] Estimated parameters are site positions and velocities at the epoch of the combination, as well as transformation parameters between each individual solution and the final combination. Using the variance component estimation method (equations A16 and A17 of *Altamimi et al.* [2002]), one variance factor per solution is estimated at each run of the CATREF combination. The combination is iterated by applying the estimated variance factors to the individual solutions included in the combination until the variance of unit weights of the combination is close to unity.

[25] We constrained velocities at colocated DORIS-DORIS, GPS-GPS, or GPS-DORIS sites to be the same since the distance between GPS or DORIS antennas at colocated sites is a few hundred meters at most. We also constrained velocities before and after discontinuities to be the same. To do so, we write that velocities of points $i$ and $j$ (colocated sites or epochs separated by a discontinuity) are constrained to be the same at a certain $\sigma$ level ($\dot{X}_i = \dot{X}_j$ , ($\sigma$)). In the multitechnique combination, the $\sigma$ of the velocity constraint is chosen as a function of the technique agreement and in such a way that the velocity normalized residuals do not exceed three.

[26] A special attention was given to the relative weight of GPS-DORIS and local ties due to an imbalance between the solutions. The GPS solution is indeed superior to the DORIS one in precision and number of stations. In addition, GPS and DORIS are global solutions by nature, whereas geodetic ties are local. As explained in more detail in *Altamimi et al.* [2011], we performed the weighting by iteratively decreasing the weight of the DORIS solution while estimating the variance factor, until a value close to unity is reached [details in *Altamimi et al.*, 2002, 2011]. We obtained variance factors of 1.2 for GPS and 1.3 for DORIS. The reference frame definition is implemented by applying minimal constraints with respect to globally distributed IGS and IDS core sites common between the ITRF2008 and the individual GPS and DORIS long-term solutions (Figure 4) using the method described in *Altamimi et al.* [2007].

[27] The resulting solution contains positions and velocities at 133 GPS sites and nine DORIS sites expressed in ITRF2008. This solution is available as Supplemental Document in tabular format (Supplemental Table 1) as well as in Solution Independent Exchange (SINEX) format with its complete variance-covariance information. The constrained velocities at collocated sites agree to within their uncertainties with formal errors less than 1 mm/yr. As expected from previous work [*Blewitt and Lavallée*, 2002], velocity uncertainties decrease rapidly after 3 years of observations (Figure 6). The best-determined sites with 8 years or more of continuous data have a formal velocity uncertainty of 0.2 mm/yr or less on horizontal velocities.

## 4. Comparison with Other Velocity Estimates

### 4.1. Methods

[28] Previous studies have shown that the scatter in GPS time series can be described by a combination of white noise and time-correlated noise with a spectral index often close to one ("flicker" noise), but more generally varying between one and two (two being "random walk" noise) [*Agnew*, 1992; *Johnson and Agnew*, 1995; *Mao et al.*, 1999; *Williams*, 2003; *Williams et al.*, 2004] . Similar results were also obtained from the noise analysis of DORIS station coordinate time series [*Le Bail*, 2006; *Williams and Willis*,

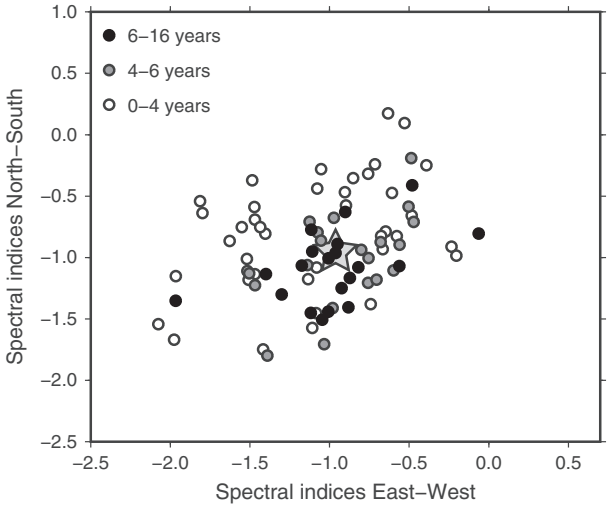


**Figure 7.** Scatter of the spectral indices of the colored noise for horizontal components of the GPS time series. The black star indicates the centroid of the scatter. It closely matches a spectral index of one for both components, indicative of flicker noise. Sites with more than 5 years of operation show a smaller scatter than younger sites.

2006]. However, the CATREF solution described above does not explicitly include time-correlated noise, which may result in overly optimistic uncertainties. We therefore compared the velocities and their uncertainties obtained from the CATREF combined solution with two other estimates (for GPS sites only).

[29] The first one uses position time series to simultaneously estimate linear terms (including offsets and slopes), nonlinear terms (annual and semiannual), and the amplitude and spectral index of a time-correlated (or power law) noise model using a Maximum Likelihood Estimation as implemented in the CATS software [*Williams*, 2008]. Given that observation, intervals at many sites are still only a few years long, these estimates may lead to somewhat optimistic uncertainties, as the most penalizing noise models (e.g., random walk noise) would take at least 5 years to identify [*Agnew*, 1992]. The resulting spectral indices for the N-S and E-W components (Figure 7) show some scatter around a centroid centered at one, indicative of flicker noise and consistent with many previous studies [e.g., *Zhang et al.*, 1997; *Calais*, 1999; *Mao et al.*, 1999; *Bock et al.*, 2000; *Williams et al.*, 2004]. We then fit flicker and white noise to all time series to estimate the slope (velocities) and their realistic uncertainties. This method works well with continuous and clean time series but has several drawbacks. First, it requires at least 4 years of continuous data collection to provide reliable spectral index estimates, while only 40% of the cGPS sites in Africa have more than 4 years of observation (Figure 3). Second, episodic time series or sites with abundant observation gaps lead to unrealistic velocity and uncertainties estimates. Finally, the method is computationally intensive, requiring up to 48 h of processing time per site for 10 years of observations on an average speed workstation.

[30] An alternative approach to estimating velocities and their uncertainties in the presence of temporally correlated noise is implemented in the GLOBK software [*Herring et al.*, 2010], with its "realistic sigma" algorithm [*Herring*, 2003; *Reilinger et al.*, 2006]. Its prime motivation is to obtain a noise model that can be implemented in a velocity solution using for instance a Kalman filter. Any First-Order Gauss-Markov (FOGM) process meets this criterion, in particular a random walk, which is used here. The method fits the increase in $\chi^2$ with successively longer averaging times to an exponential function (as expected from a FOGM process), then evaluates the exponential function at infinite averaging time to get the velocity uncertainty. This method is computationally efficient and can handle time series with outliers and data gaps.

### 4.2. Results

[31] Figure 8 compares horizontal velocity estimates among the three solutions described above. We find that they agree well, with mean differences of 0.1±0.5 mm/yr or better and maximum differences of 3 mm/yr. We find two significant outliers at ROBE (Ethiopia) and ASMA (Eritrea). Robe is a young site, with only 2.5 years of continuous observations and shows nonlinear displacements that are unlikely tectonic in origin. Asma shows numerous

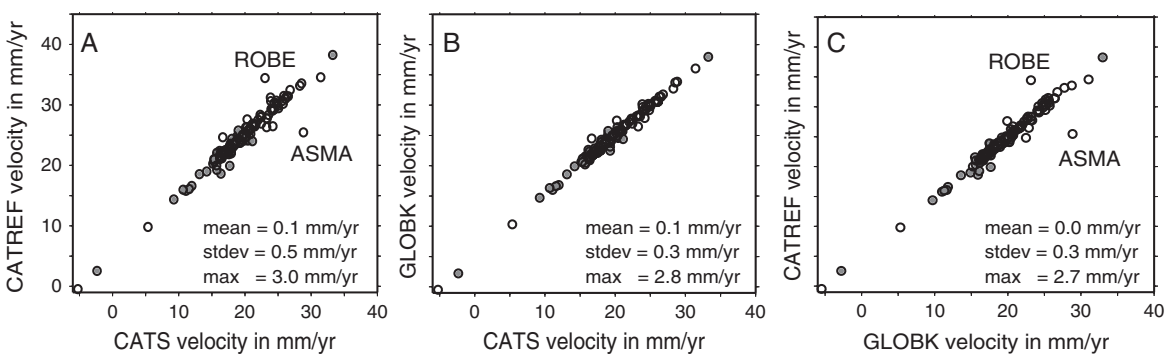


**Figure 8.** Comparison of site velocities estimates between CATREF, CATS, and GLOBK (explanation in the text). Only GPS sites common to both solutions are shown. Gray circles show the NS component, and open circles show the EW component. Mean, stdev, and max are the mean, standard deviation, and maximum value of the difference between two solutions. Outliers ROBE and ASMA have been omitted from the values provided on Figures 8A and 8C.

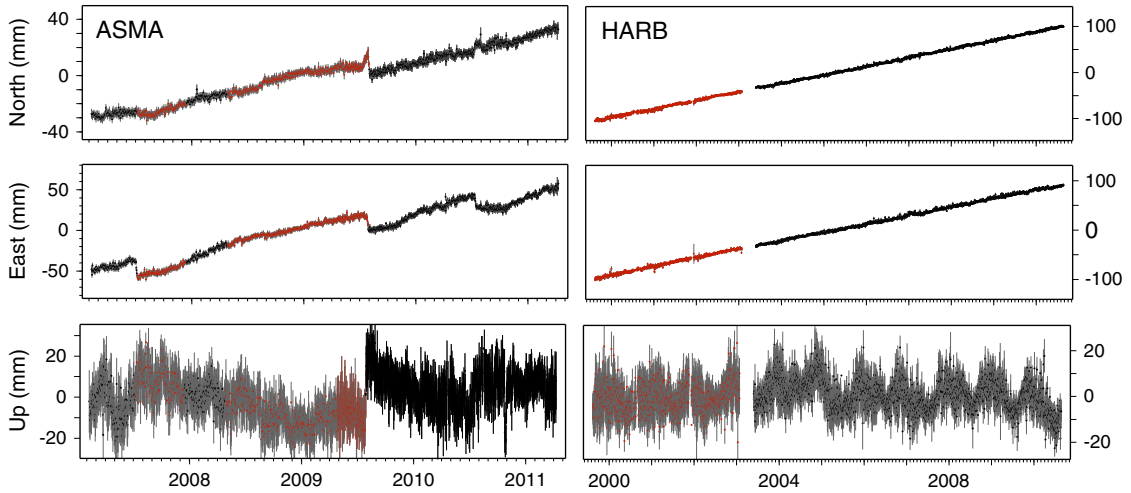


**Figure 9.** Selected GPS position time series for sites ASMA (Asmara, Eritrea) and HARB (Hartebestoek, South Africa). Alternating black and red dots show positions on either side of a documented equipment change of any unexplained offset in the time series. HARB is one of the cleanest and most continuous time series of all sites in Africa, while ASMA shows numerous problems.

unexplained and undocumented jumps (Figure 9), although the site log-sheet shows that the site monument is a concrete pillar on a clay soil. These jumps may reflect poor monument quality, local tectonic or magmatic activity, or equipment-related issues.

[32] Figure 10 compares velocity uncertainties among the three solutions described above. We find that the GLOBK and CATS solutions agree better on average (within 0.25 mm/yr) than the CATS-CATREF (0.60 mm/yr) or GLOBK-CATREF solutions (0.50 mm/yr). The fact that CATREF uncertainties are systematically lower than their GLOBK or CATS counterparts is consistent with the fact that CATREF does not explicitly account for colored noise, as noted above. CATREF uncertainties only depend on the uncertainties of individual solutions and on the internal agreement between consecutive weekly solutions, determined by the variance factor between solutions estimated in the combination (see above). We therefore decided to scale the CATREF velocity uncertainties to make them consistent with the CATS and GLOBK ones, which formally include colored noise. To do so, we computed a scaling factor that, when applied to CATREF uncertainties, best matches the CATS and GLOBK ones (Figure 10). We found a scaling factor of 1.5, which we subsequently applied to all velocity uncertainties from the CATREF solution.

[33] Most IGS sites benefit from a well-documented and stable geodetic monument as they are installed for high-precision geodetic and geophysical applications. Other sites were installed for various purposes, including surveying, meteorological, or ionospheric studies. Their monumentation quality is not always known and may not adhere to IGS standards for stability, except for those installed for high-precision geodetic and geophysical applications. Since monument instability is one of main sources of time-correlated noise in geodetic measurements [*Wyatt*, 1989; *Johnson and Agnew*, 1995; *Langbein et al.*, 1995; *Langbein and Johnson*, 1997], this must be accounted for before interpreting the results and deciding on the site list that will constitute the frame of reference for Africa. We therefore ranked GPS monuments as category A (sites on strong concrete pillars or still pins on bedrock outcrops), B (sites on shallow foundation and roof of buildings), C (sites on fence poles or cadastral beacons), and U (unknown monument type). This ranking, although some-

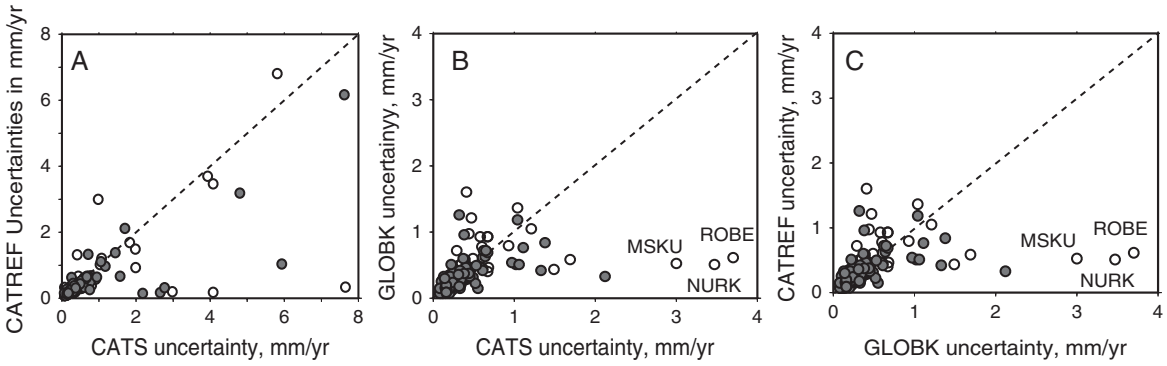


**Figure 10.** Comparison of velocity uncertainties. CATREF uncertainties have been multiplied by 1.5, as explained in the text. Only GPS sites common to two solutions are shown. Gray circles show the NS component, and open circles show the EW component.

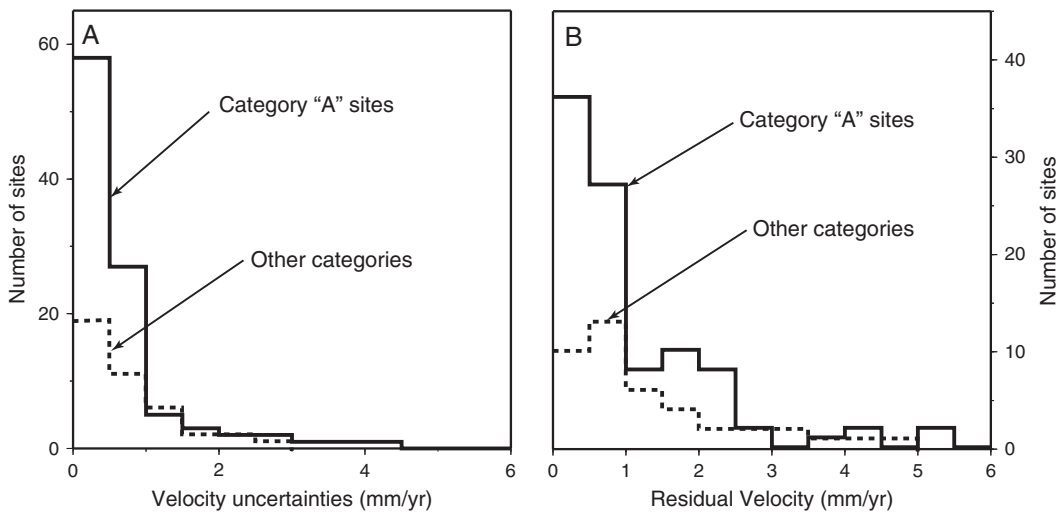


**Figure 11.** Distribution of GPS site (A) velocity uncertainties and (B) residual velocity. Solid line shows category A sites, and dashed line shows other sites. Overall, category A sites perform significantly better than others.

what subjective, nonetheless, provides information about the expected long-term stability of GPS monuments and hence the reliability of the associated positions and velocities. Figure 11 compares velocity uncertainties and residual velocities in a plate-fixed frame with monument quality as defined above. As expected, we find that category A sites perform significantly better than other categories, with by far the smallest velocity uncertainties and residual velocities. This reinforces the need for high-quality monumentation for geophysical applications in Africa and elsewhere.

## 5. Discussion

### 5.1. Definition and Rigidity of the Nubian Plate

[34] Large earthquakes and major active tectonic features in Africa concern mostly its northern edge, with the oblique convergence between Nubia and Eurasia, and its eastern edge, with the divergence between Nubia and Somalia in the East African Rift (Figure 1). The Nubian plate itself, however, is not devoid of active deformation features, as indicated by active volcanism along the Cameroon line [*Moreau et al.*, 1987; *Ubangoh et al.*, 1997; *Tokam*, 2010] or significant earthquakes outside of the main plate boundaries [*Njome et al.*, 2010; *Tedesco et al.*, 2007], including those marking the propagation of rifting into Zambia, Zimbabwe, and Botswana (Luangwa, Mweru, and Upemba grabens). Current deformation rates across these active structures are probably small, given that they are not marked by prominent topography, but they are unknown. Determining the current level of intraplate deformation—or lack thereof—in Nubia is important to better quantify the potential hazard posed by these active structures as well as to precisely determine a plate-fixed frame for geodetic applications in Africa. The challenge is the lack of a dense, homogeneous continuous GPS network over most of Africa, in contrast to other plate interiors such as Western Europe [e.g., *Nocquet et al.*, 2001] or North America [e.g., *Calais et al.*, 2003] .

[35] We therefore seek to objectively determine the set of GPS sites that best defines rigid Nubia, following the method developed by *Nocquet and Calais* [2003] . We start by solving for Nubia's angular velocity with respect to ITRF based on all sites located on the stable part of the plate with an observation time span of at least 2.5 years and horizontal velocity uncertainties less than 1.5 mm/yr. We define "stable Nubia" using the geologic criteria defined by *Argus and Gordon* [1996], i.e., we exclude sites close enough to major active faults or large historical earthquakes to be affected at the 1 mm/yr level by elastic strain accumulation or coseismic deformation. This represents a total of 94 sites. To find the best set of sites that defines rigid Nubia, we then iteratively remove one site at a time and use an F-ratio test to determine whether the fit to a rigid plate model is statistically better without that particular site [*Stein and Gordon*, 1984; *Nocquet et al.*, 2001]. The F-ratio is defined as follows:

$$F = \frac{\left[\chi^2_{p_1} - \chi^2_{p_2}\right] \Big/ (p_1 - p_2)}{\chi^2_{p_2} \Big/ p_2} \tag{5}$$

[36] This F-ratio compares an estimate with $p_1$ degrees of freedom ($p_1 = n\times2 - 3$) where $n$ is the total number of sites considered to an estimate with $p_2$ degrees of freedom ($p_2 = (n-1)\times2-3$). The F-ratio is used to determine whether the increase in $\chi^2$ from the estimate with $p_2$ degrees of freedom to the estimate with $p_1$ degrees of freedom ($p_1 > p_2$) is significant at a given risk (or confidence) level. This ratio is then compared to the expected value of a $F(p_1 - p_2, p_2)$ Fisher-Snedecor distribution for a risk level $\alpha$ (i.e., $100 - \alpha$ corresponding to 95% or 99% confidence level) as follows:

$$F \leq f_{\alpha^{p1-p2,p2}} \tag{6}$$

where $f_{\alpha^{p1,p2}}$ is the $\alpha$% fractile for Fisher-Snedecor law with $(p_1, p_2)$ degrees of freedom. If this equation is not satisfied, then the site velocity is not consistent with the rigid rotation estimates using all the other sites, with a risk of $\alpha$% of being incorrect (or a confidence of $100 - \alpha$% of being correct).

[37] Supplemental Table 2 shows the results of this procedure for the sites used here on the Nubian plate (threshold values are provided in Supplemental Table 3). It also shows the results of a more conventional $\chi^2$ test and of the Student test, described in more detail in *Nocquet et al.* [2001]. We chose to be conservative and define Nubia using only sites that pass the F-ratio test and at least one of the Student or $\chi^2$ tests. This leaves a subset of 51 sites. We further refined the site selection by searching for the subset of sites that results in a reduced $\chi^2$ of the Nubia angular estimate close to unity. This leaves a subset of 40 sites on the Nubian plate whose velocities agree with a rigid plate model with a reduced chi-squared of 1.2 (GPS sites ANTH, BENI, BWES, DEAR, DRBN, ELDN, ETJI, GDAL, GMAS, GOUG, GRHM, HEID, INHB, KLEY, KMAN, KSTD, LSMH, MAS1, MBRY, MFKG, NIAM, NKLG, NSPT, NYLS, PMBG, PSKA, QTWN, RBAY, RECT, SBOK, SHEB, STBS, SUTH, SUTM, UMTA, UPTA, VERG, YKRO, plus DORIS sites hbka and licb, Figure 16). This is the largest set of sites used so far to define stable Nubia. We also tested using sites that pass the more conventional $\chi^2$ test only (i.e., formally expressing that a velocity is significant if it lies outside of its error ellipse at a given confidence level), which results in a subset of 60 sites and provides very similar results. The weighted root-mean-square residual with respect to a rigid plate model for that subset of sites is 0.6 mm/yr, with values less than 1 mm/yr (Figure 12). This is consistent with the level of rigidity found for other major plates such as Eurasia [*Kogan and Steblov*, 2008], North America [*Dixon et al.*, 1996; *Calais et al.*, 2006a], or Australia [*Tregoning*, 2003] . This does not preclude deformation larger than 1 mm/yr at a local or regional scale, as the 40 sites used here to define stable Nubia, although they extend across the entire continent, have a very uneven spatial coverage and do not sample large portions of Africa. Parts of Nubia with dense cGPS networks such as Benin and its surroundings or South Africa also show insignificant velocity residuals (maximum 0.8 mm/yr).

[38] The best-fit angular velocity of Nubia with respect to ITRF2008 (Table 1 and Figure 13) is close to the recent estimate of *Altamimi et al.* [2012]. The associated uncertainty is however smaller in the solution presented here, most likely because of the larger number of sites used here to define Nubia (40 sites, as opposed to 11 in *Altamimi et al.* [2012]). The uncertainty associated with this new angular rotation of Nubia with respect to ITRF are the smallest so far, most likely because the solution presented here is based on a larger number of geodetic sites and longest observation time span. Both Euler poles are however shifted southward by about 2° compared to previously published solutions for the angular rotation between Nubia and ITRF, which are all based on previous realizations of ITRF (from ITRF2000 to ITRF2005) [*Altamimi et al.*, 2002, 2007]. We suspect that this reflects recent changes in the definition of the ITRF in its most recent release, ITRF2008 [*Altamimi et al.*, 2011].

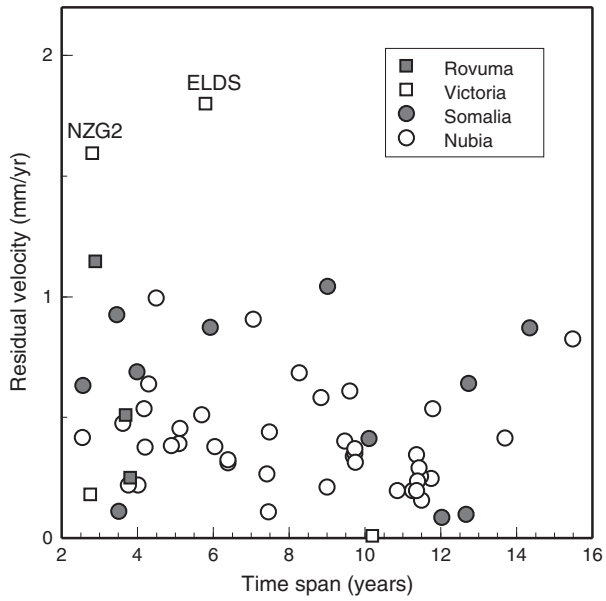


**Figure 12.** Residual velocities with respect to a rigid plate model for the sites used in the definition of Nubia, Somalia, Victoria, and Rovuma. Residual velocities range between 0 and 1 mm/yr, consistent with the velocity uncertainties, except for two sites on the Victoria plate. There is a weak correlation between observation time span and residual velocity for Nubia plate sites.

[39] Residual velocities with respect to stable Nubia as defined above (Figure 14) illustrate regions with significant active deformation. Large residuals at all sites located east of the East African Rift are to be expected, as this region includes the Somalian plate and other smaller plates (Figure 1). This is analyzed in more detail below. We also find significant deviation from plate rigidity at sites RABT, IFRN, and TETN in Morocco (residual velocities directed SSE at 1.0 mm/yr, 1.3 mm/yr, and 1.5 mm/yr, respectively).

**Table 1.** Angular Velocity Estimates From This Study[a].

| Moving | Reference | Degrees | | deg/My | | Error Ellipse, Deg. | | | Covariance ($10^{-10}$ rad$^2$/My$^2$) | | | | | |
|---|---|---|---|---|---|---|---|---|---|---|---|---|---|---|
| Plate | | Lat | Lon | $\omega$ | $\sigma_\omega$ | $S_{maj}$ | $S_{min}$ | azim | $c_{xx}$ | $c_{xy}$ | $c_{xz}$ | $c_{yy}$ | $c_{yz}$ | $c_{zz}$ |
| Nubia | ITRF08 | 49.35 | –80.78 | 0.265 | 0.000 | 0.6 | 0.3 | 92.0 | 1.2 | –0.1 | 0.3 | 3.5 | 0.7 | –0.9 |
| Somalia | Nubia | –39.38 | 36.64 | 0.062 | 0.002 | 6.6 | 4.1 | 147.0 | 15 | –16 | 18 | 1 | 8 | 7 |
| Victoria | Nubia | 5.86 | 31.73 | –0.154 | 0.032 | 15.3 | 12.2 | 54.1 | –63 | 665 | –71 | 375 | –271 | 3151 |
| Rovuma | Nubia | –18.96 | 36.21 | 0.118 | 0.045 | 19.1 | 17.4 | 133.7 | 148 | –3211 | 3103 | 439 | 370 | 6136 |

[a]Lat and lon are the latitude and longitude of the euler pole, $S_{maj}$, $S_{min}$, and azim are the semimajor axis, semiminor axis, and Azimuth (clockwise from north) of the corresponding error ellipse (95% confidence). $\omega$ is the angular rotation rate and $\sigma_\omega$ its uncertainty. $c_{xx}$, $c_{xy}$, $c_{xz}$, $c_{yy}$, $c_{yz}$, and $c_{zz}$ are the upper triangular elements of the corresponding variance-covariance matrix in cartesian coordinates.

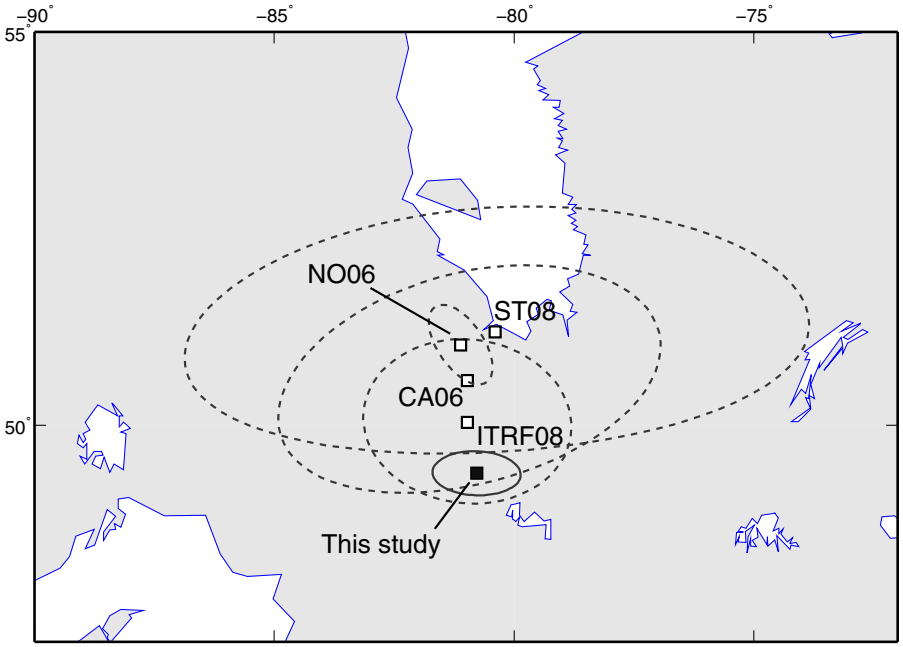


**Figure 13.** Map view of location and uncertainty of the Nubia-ITRF2008 rotation pole estimated here (solid line) and determined in other recent studies (dashed lines). Error ellipses are 95% confidence. ITRF08 = *Altamimi et al.* [2012]; ST08 = *Stamps et al.* [2008]; CA06 = *Calais et al.* [2006b]; NO06 = *Nocquet et al.* [2006]. Our result plots close to the ITRF2008 solution.

This is consistent with previous results based on campaign GPS observations [*Fadil et al.*, 2006] and interpreted by these authors as the surface expression of the roll back of a delaminated subcontinental slab beneath the Rif Mountains. We note the smaller residual at station RABT, perhaps reflecting the fact that the site is located outside of the deformation zone [*Argus et al.*, 2011], with a direction collinear to those of TETN and IFRN. Residual velocities at sites MAS1 and GMAS, although not statistically different from zero, are also in that same direction, perhaps suggesting a wider impact of the deformation mechanism responsible for motions of TETN and IFRN. The large residual velocity at site DAKA (∼1.0 mm/yr) is due to repeated offsets and gaps in the position time series. The site is installed on a building top on unconsolidated sediments. We hypothesize that the installation setup and perhaps some equipment issues are responsible for its poor quality time series.

[40] *Mantovani et al.* [2007] used spreading rates, transform azimuths and onland deformation features to postulate the existence of a Morocco microplate separate from Nubia. In their hypothesis, GPS sites LPAL, GMAS, and MAS1 lie on the Morocco microplate (or within the boundary between Morocco and Nubia for the latter two). Supplemental Table 2, which displays how well GPS sites fit our best Nubia plate rotation, shows that GMAS and MAS1 pass all the tests and LPAL passes the $\chi^2$ and F-ratio test. Therefore, the data does not appear to require an additional Morocco microplate. We also used an F-ratio test to determine whether the decrease in $\chi^2$ from an angular velocity estimate assuming a single Nubian plate (null hypothesis) to one that assumes a Morocco microplate (defined by sites LPAL, GMAS, and MAS1) separate from Nubia is significant. We find that it is not the case, with a confidence level greater than 99%. Finally, we tested whether velocities predicted by *Mantovani et al.* [2007] at sites on the postulated Morocco microplate (LPAL, MAS1, and GMAS) could explain the observed residual velocities with respect to Nubia at those sites. We calculated those residuals by omitting sites LPAL, MAS1, and GMAS from the Nubia angular velocity estimation. We find that the predicted velocities are three times larger than the observed residuals and in a direction opposite from the observed ones, as also reported by *Argus et al.* [2010]. We conclude that the data set used here excludes the hypothesis of a Morocco microplate separate from Nubia proposed by *Mantovani et al.* [2007].

[41] The GPS data set used here is currently insufficient to test whether there is significant relative motion across the seismic zones that separate Africa's large cratons (West African, Congo, Kalahari). We note, however, a general SSE-NNW convergence between residual velocities in the northern and southern parts of stable Nubia (Figure 14). We used an F-ratio test to quantify whether the velocity field is better fit by a single plate or by two separate plates with a boundary along the Cameroon Volcanic Line and Central Africa shear zone. We defined northern Nubia using sites ETJI, GMAS, NIAM, RECT, TAMP, and YKRO, and southern Nubia using sites DEAR, hbka, HNUS, GOUG, INHB, LLNG, PRE1, RBAY, SBOK, SUTH, SUTM, ULDI, UMTA, and ZAMB. We found that the decrease in $\chi^2$ from a 1-plate to a 2-plate model is not significant at the 95% confidence level. Therefore, the apparent systematic difference in residual velocities between northern and southern Africa is not sufficient, at this point, to justify splitting Nubia into two subplates. A longer observation time span and additional cGPS sites in Africa are needed to further confirm this hypothesis.

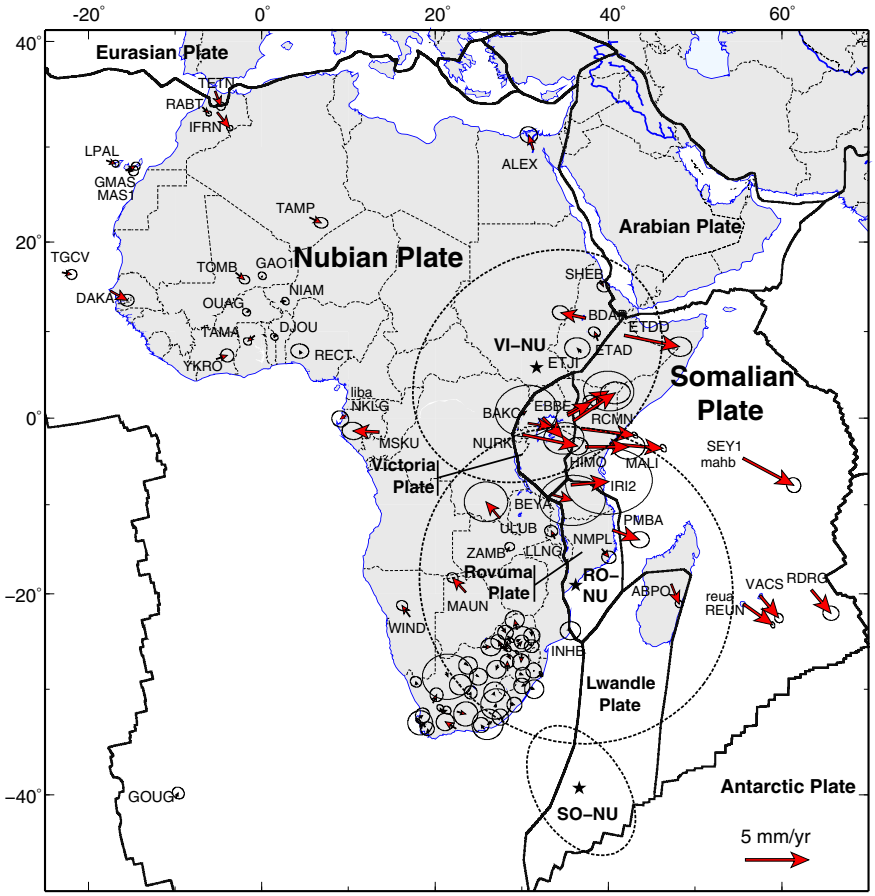


**Figure 14.** Velocity solution with respect to Nubia. For sake of readability, we are only plotting sites with velocity uncertainties less than 1.5 mm/yr. Site velocity error ellipses are 95% confidence. Stars show the Euler poles and their associated 95% confidence error ellipse for Somalia-Nubia, Victoria-Nubia, and Rovuma-Nubia (values in Table 1).

### 5.2. Kinematics of the Somalian Plate

[42] The relative motion between the Nubian and Somalian plates sets the kinematic boundary condition across the East African Rift. Space geodetic instrumentation on the Somalian plate is very sparse (Figure 1), because of its largely oceanic nature and of the logistical difficulties to install sustainable geophysical equipment in some regions of eastern Africa. Previous estimates of the relative motion between Somalia and Nubia relied on three IGS sites SEY1, REUN, MALI [*Sella et al.*, 2002; *Prawirodirdjo and Bock*, 2004; *Altamimi et al.*, 2012]. To better constrain their results, some studies used additional kinematic information such as earthquake slip vectors [*Calais et al.*, 2006b] or a plate circuit closure condition with Antarctica including magnetic anomalies and transform faults direction along the South West Indian Ridge [*Horner-Johnson et al.*, 2007; *Stamps et al.*, 2008].

[43] Thanks to newly installed GPS sites on the Somalian plate (e.g., sites ROBE, ETDD, DAMY, RCMN, MAL2, VACS, and RDRG), along with longer observation time spans at IGS sites SEYI, REUN, MALI, and DORIS sites reua and mahb, we are now in a position to more accurately determine the relative motion between Somalia and Nubia based on geodetic data alone. We defined the Somalian plate starting with all continuous GPS sites, plus episodic GPS sites HIMO, ARS1, LGDO, and DORIS sites reub, reua, and mahb. As explained above for Nubia, we removed sites one by one and tested their consistency with a rigid Somalian plate using an F-ratio test (Supplemental Table 2). We paid particular attention to sites located close to tectonically and/or volcanically active structures. We found that all GPS sites on the volcanically active Reunion island have velocities that are consistent with rigid Somalia and could therefore be used to define its kinematics. Site ETDD, located 50 km east of the actively extending Main Ethiopian Rift, is also consistent with rigid Somalia. Sites ROBE and DAMY, located 15 and 20 km from the rift, fail the F-ratio test and are therefore inconsistent with rigid Somalia (with residual velocities of 1.8 and 2.2 mm/yr, respectively). We therefore discarded those two sites from the definition of the Somalian plate. Site ABPO, located in central Madagascar within a region of extensional seismicity [*De Wit*, 2003] that may constitute the diffuse boundary between the Lwandle and Somalian plates [*Horner-Johnson et al.*, 2007], also fails the F-ratio test, with a residual velocity of 1.4 mm/yr with respect to Somalia. Finally, we removed site ARS1 from the definition of Somalia because of its large residual (1.7 mm/yr) although its large uncertainty allows the site to pass all statistical tests. Site ARS1

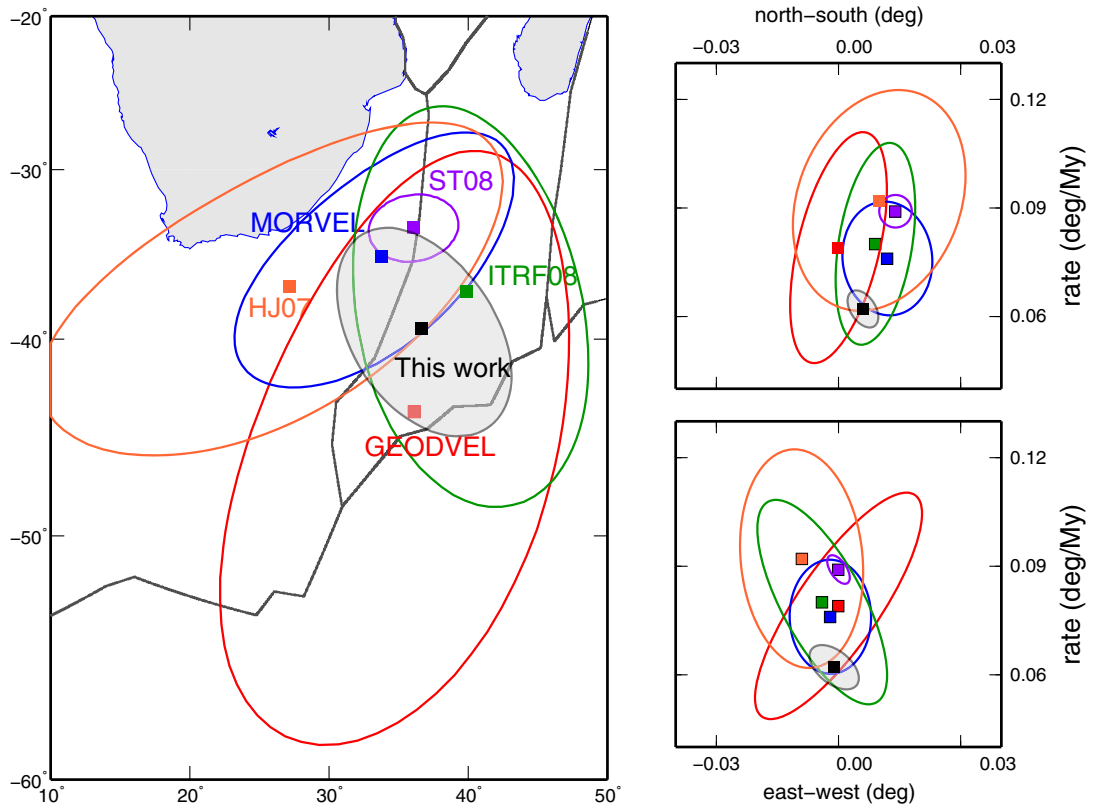


**Figure 15.** Angular velocities for Nubia-Somalia and 95% confidence limits in three perpendicular planes. Left panel = rotation poles, bottom right-hand panel = profile from west to east, and top right-hand panel = profile from south to north. Our best estimate is compared to recent solutions by *Horner-Johnson et al.* [2007] (HJ07), *Stamps et al.* [2008] (ST08), *Argus et al.* [2010] (GEODVEL), *DeMets et al.* [2010] (MORVEL), and *Altamimi et al.* [2012] (ITRF08).

is located at close distance to major active volcanoes (Kilimanjaro and Meru) and to the active Pangani rift fault [*Le Gall et al.*, 2007]. The final list includes nine sites (GPS sites ETDD, HIMO, LGDO, MALI, MOSH, REUN, SEY1, and DORIS sites reua and mahb) with a mean weighted residual of 0.7 mm/yr and residuals less than 1 mm/yr (Figures 12 and 16).

[44] Table 1 and Figure 15 compare our resulting Nubia-Somalia angular velocity with recently published estimates. We focus the discussion on the most recent and best-determined angular velocities [*Stamps et al.*, 2008; *DeMets et al.*, 2010; *Argus et al.*, 2010; *Altamimi et al.*, 2012] as other estimates are based on much fewer observations. In addition, *Argus et al.* [2010] and *Altamimi et al.* [2012] have the advantage that they do not assume the translational velocity of the reference frame to be that of ITRF. Our Euler pole lies within the cluster of these recently published estimates (Figure 15), and its 95% confidence interval includes the best estimates from *DeMets et al.* [2010, MORVEL], *Argus et al.* [2010, GEODVEL], *Altamimi et al.* [2012, ITRF08], and (barely) *Stamps et al.* [2008]. We however found a Nubia-Somalia rotation rate that is 25% slower than previous estimates, although consistent with them (except that of *Stamps et al.* [2008]) at the 95% confidence level. We tested whether this difference in rate could be due to the fact that our estimate does not account for a translational velocity of the reference frame. To do so, we added the frame translation rate values calculated by *Altamimi et al.* [2012] ($\dot{T}_x$, $\dot{T}_y$, $\dot{T}_z$ equal 0.41, 0.22, and 0.41 mm/yr, respectively) to the observed GPS and DORIS velocities and solved for a Nubia-Somalia angular velocity. This shifts the Euler pole eastward by about 5° but has no significant impact on the rotation rate. We also tested defining Somalia using only the three "historical" sites with the longest times series (MALI, REUN, and SEY1; the same set as used by *Argus et al.* [2010]). The angular velocity is essentially unchanged, with a rotation rate that is still slower than previously published estimates. The reason for this difference in rotation rate remains to be investigated further. It could stem from the version and implementation of the geodetic reference frame used here, and/or from the accuracy of the geodetic velocities, which increases with time series duration.

[45] Our Somalia-Nubia angular velocity estimate implies a divergence rate of 5 mm/yr in the Main Ethiopian Rift, decreasing southward to about 4 mm/yr at the latitude of Tanzania, and 3 mm/yr at the latitude of northern Mozambique (Figure 17). These rates and divergence directions are similar, within uncertainties, to those predicted by MORVEL [*DeMets et al.*, 2010] and by *Stamps et al.* [2008], two studies that use 3.16 Ma average geological data. This consistency between geologic and geodetic data indicates that the Somalia-Nubia relative motion has remained steady

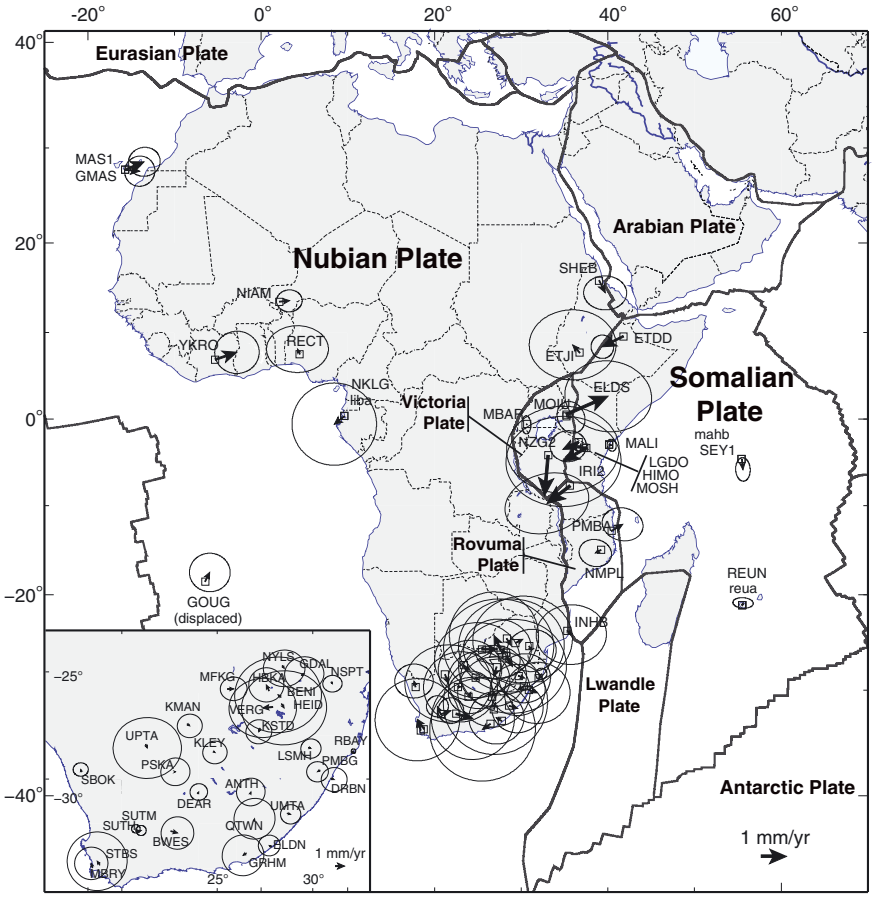


**Figure 16.** Sites used to define the Nubia, Somalia, Victoria, and Rovuma plates and their residual velocities, shown with their 95% confidence error ellipse. Note that site GOUG has been moved from its actual position at [lon= –9.88, lat= –40.35] in order to be visible. Inset at the bottom left shows a zoom on the South African (TRIGNET) sites.

over the past 3 Myr, a result that confirms *Stamps et al.*'s [2008] finding and holds for most major plates [e.g., *Sella et al.*, 2002].

### 5.3. Kinematics of the East African Rift

[46] *Hartnady* [2002] used seismicity and active faults in the EAR to first propose that this major boundary included additional microplates, including Victoria, Rovuma, and Lwandle (Figure 1). *Calais et al.* [2006b] tested this hypothesis and used geodetic data and earthquake slip vectors to estimate the angular rotation of Victoria with respect to Nubia. *Stamps et al.* [2008] used a slightly augmented geodetic data set, added 3.2 My average oceanic data along the Southwest Indian Ridge [*Horner-Johnson et al.*, 2007], and a plate circuit closure condition with Antarctica to refine the kinematics of Victoria and determine that of the Rovuma and Lwandle microplates. However, their angular velocity estimates for Rovuma and Lwandle were poorly constrained, as they did not include geodetic data on either of them. There is now access to enough GPS stations in East Africa to solve for the angular velocity of the Victoria and Rovuma microplates using geodetic data alone. A caveat remains regarding the definition of the boundaries between these microplates. Here we used those defined in *Stamps et al.* [2008] but caution that further geological work is needed to more accurately define them.

[47] We defined the Victoria plate using the method presented above for the Somalia-Nubia relative motion. We first inverted horizontal velocities at all GPS sites with observation time span larger than 2.5 years located in the interior of the Victoria plate. Seven continuous GPS sites (BAKC, EBBE, ELDS, MBAR, MOIU, NJOR, and NURK) and two episodic sites (KIOM and NZG2) fulfill that criterion. An F-ratio test shows that cGPS sites BAKC (likely experiencing elastic strain accumulation on the active faults bounding the Ruwenzori mountains) and NURK, as well as episodic site KIOM are inconsistent with a rigid Victoria plate model. In addition, we found that sites EBBE and NJOR must be removed from the plate definition in order to obtain a reduced $\chi^2$ close to unity. This leaves only four sites (ELDS, MBAR, MOIU, and NZG2), whose velocities fit a rigid plate model with a reduced $\chi^2$ of 1.2. Residual velocities range from 0.1 to 1.9 mm/yr (Figures 12 and 16), within the uncertainties of the input data, but are significantly larger than for other plates. The resulting Victoria-Nubia Euler pole is located north of the Victoria plate, with an angular rate defining a counterclockwise rotation with respect to Nubia (Figure 18). This Euler pole is consistent, within uncertainties (95% confidence), with those of *Calais et al.*

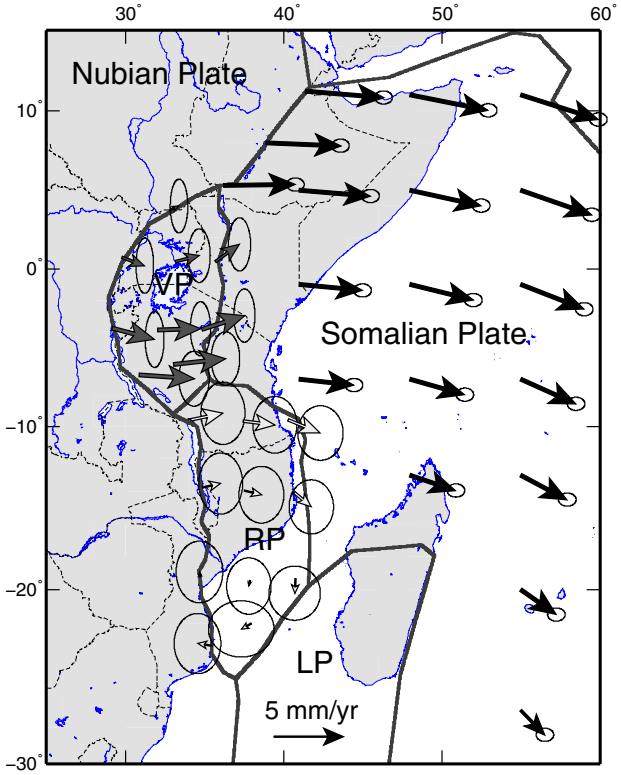


**Figure 17.** Predicted velocities with respect to Nubia for the Somalia, Victoria, and Rovuma plates (with 95% confidence error ellipse) using angular velocities provided in Table 1. VI: Victoria plate, RO: Rovuma plate, LW: Lwandle plate.

[2006b] and *Stamps et al.* [2008]. However, its uncertainty is significantly larger than previous estimates, even though we are now using more sites with longer position time series. This result, in addition to the large velocity residuals and the small percentage of sites fitting a rigid Victoria plate model may indicate that the plate is not as rigid as previously thought or that the geodetic data is still insufficient to accurately determine its angular velocity.

[48] We defined the Rovuma plate starting with cGPS sites PMBA and NMPL in Mozambique and episodic GPS sites BEYA, IRI2, and MAK2 in southern Tanzania. An F-ratio test shows that all five site velocities are consistent with a rigid block model (Supplemental Table 2), with a reduced $\chi^2$ of 1.6. Residuals velocities range from 0.4 to 1.2 mm/yr, consistent with the data uncertainty (Figure 12 and 16). We found that the kinematics of the Rovuma plate is described by a clockwise rotation with respect to Nubia. Our estimate encompasses that of *Stamps et al.* [2008], which only uses earthquake slip vector directions and one episodic site in southern Tanzania, but has a large uncertainty because of the small number of sites used here and the poor geographic coverage of the plate. The Rovuma-Nubia relative motion found here implies a maximum divergence of about 4 mm/yr in the northern part of the plate, decaying rapidly to the south (Figure 17). Uncertainties on predicted velocities are however large, a consequence of the small number of sites used to constrain the Rovuma angular velocity.

[49] We also tested whether the data is better fit by a Rovuma microplate separate from Somalia or by a single Rovuma+Somalia plate using an F-ratio test [*Stein and Gordon*, 1984]. We used the GPS and DORIS sites listed above to define Rovuma and Somalia. We find that the decrease in $\chi^2$ from a one-plate model (null hypothesis, $\chi^2 = 50.3$) to a two-plate one ($\chi^2 = 3.2$) is significant at the 99% confidence level ($F_{ratio} = 59.9$, while for $\alpha = 0.01$ $f_{\alpha 3,12} = 5.95$). This indicates that the data is better fit with Rovuma separate from Somalia.

### 5.4. Vertical Velocities

[50] It is well known that the vertical component of GPS positions and velocities is not as accurately or precisely defined as the horizontal [e.g., *Švábenský and Weigel*, 2004; *Nocquet et al.*, 2006]. However, several studies have shown that continent-wide vertical velocities could be determined that match predictions from geophysical models at the mm/yr level. For instance, it is now well established that vertical velocities in North America primarily reflected

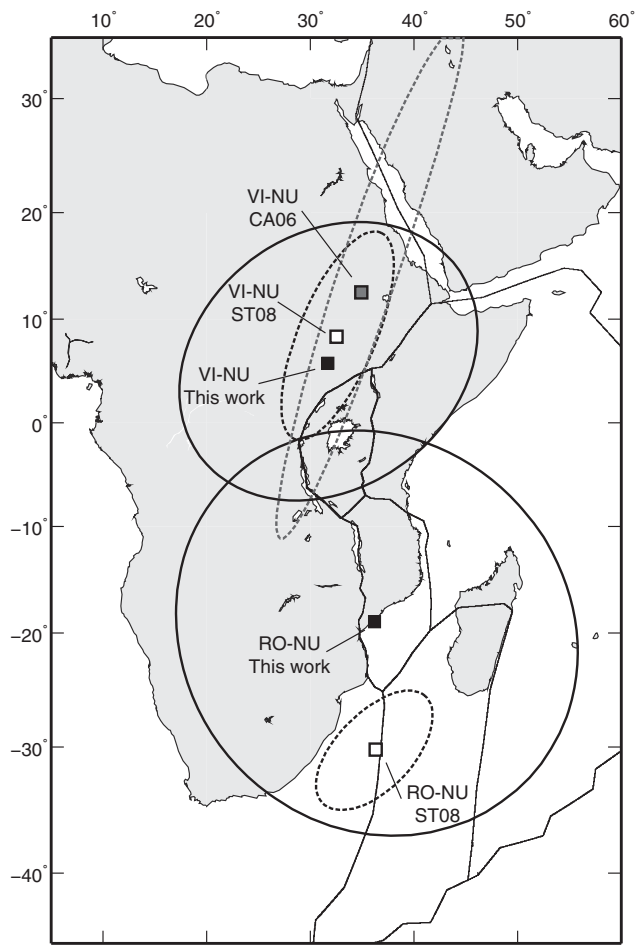


**Figure 18.** Map view of the location and uncertainty of the Victoria-Nubia (VI-NU) and Rovuma-Nubia (RO-NU) rotation poles estimated here (black square and solid line error ellipse) and determined in other studies (white and grey squares, dashed error ellipses). Ellipses are 95% confidence. CA06 = *Calais et al.* [2006b]; Sta08 = *Stamps et al.* [2008].

the effects of Glacial Isostatic Adjustment (GIA) following the melting of large ice sheets between 16 and 10 thousand years ago [*Argus et al.*, 1999; *Calais et al.*, 2006a; *Sella et al.*, 2007; *Argus and Peltier*, 2010]. The contribution of GIA in Africa is negligible, but other nontectonic processes such as hydrological or atmospheric loading [e.g., *van Dam et al.*, 2001] or local processes such as water withdrawal can significantly affect vertical positions.

[51] Hydrological and atmospheric loading are largely dominated by seasonal signals that can reach up to 30 mm of vertical displacement peak-to-peak. Although these seasonal signals may be large, they average out over time so that their effect on vertical velocity estimates is negligible after 2.5 years of continuous measurements [i.e., *Blewitt and Lavallée*, 2002]. However, poroelastic effects induced by groundwater withdrawal (e.g., draining from large water bodies or pumping from a borehole for irrigation) typically contain interannual variations that may have an impact on vertical velocities. For instance, *Argus et al.* [2005] showed that the Santa Ana aquifer of metropolitan Los Angeles is subsiding at about 3 mm/yr due loss of water resources. Similar processes may well affect Africa, for instance through the draining of water from Lake Victoria to the Nile River [i.e., *Awange et al.*, 2009] or the massive borehole pumping of water from aquifers in southern Africa. These regional signals are difficult to identify and filter out in areas with sparse geodetic instrumentation such as most of Africa. Although the effect on vertical surface motions and their geographic extent of the areas impacted remain to be quantified, these signals may well contribute to the vertical velocities determined in this study.

[52] Finally, one may expect vertical signals in Africa caused by large-scale tectonic activity or magmatic processes. The latter should be concentrated on the East African Rift, in particular along the volcanically active Main Ethiopian rift and Eastern (Kenyan) Branch. The former may affect a broader region via the impact of the African Superplume [*Nyblade and Robinson*, 1994] although mantle flow models indicate that its impact on present-day vertical velocities does not exceed 0.12 mm/yr [*Gurnis et al.*, 2000; *Moucha and Forte*, 2011] .

[53] The vertical velocities found in this study range from –2 to +2 mm/yr (Figure 19). As expected, uncertainties rapidly decrease with time (Figure 6) from ∼1 mm/yr after 4 years of observations to less than ∼0.5 mm/yr after 10 years. There is no apparent correlation between observation time span and vertical velocity, although sites with more than 12 years of continuous operations all have low vertical velocities, similar in magnitude to their uncertainty. We also find a weak correlation between vertical velocities and their uncertainties (Figure 20).

[54] Moreover, vertical velocities in map view (Figure 19) are difficult to interpret because of the low density of stations in most of Africa. We do observe positive vertical velocities over most of continental Nubia, with up to 1.8±0.6 mm/yr at Windhoek, Namibia. However, the continent is largely undersampled, and this work likely misses a variability still to be discovered. For instance, vertical velocities in South Africa, the only densely instrumented region, indicate close to zero vertical motion over most of the network, except for a subset of regionally consistent positive vertical velocities (up to 1.5 mm/yr) in its northeastern part.

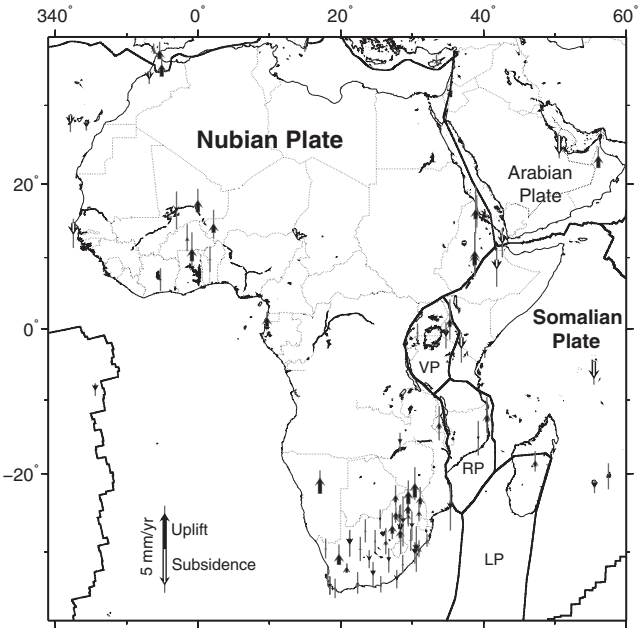


**Figure 19.** Vertical velocities with respect to ITRF2008 derived from this study. For the sake of readability, we only show sites with uncertainties less than 1.5 mm/yr. Open arrows show subsidence, and black arrows show uplift.

### 5.5. Implication for an African Reference Frame

[55] Our study provides a number of contributions to the definition of an African Reference Frame as recommended by the AFREF initiative [*Wonnacott*, 2005, 2006]. Most practical applications prefer that the frame be tied to Africa and static, i.e., defined by fixed station coordinates at a given epoch. Here we show that the interior of the Nubian plate is rigid at the 0.6 mm/yr level, an upper bound for intraplate deformation that is consistent with other continental interiors. When carried forward in time, it would take about 30 years for deformation to accumulate to a level detectable by precise surveying applications, assuming they are precise to 2 cm in horizontal, a precision typically reached by surveyors nowadays, although GPS precision will likely continue to increase in the future for surveying applications. Also, a longer observation time span and a higher spatial density of well-distributed cGPS sites will allow us to refine the estimate of Nubia's rigidity in the future. However, the low level of intraplate deformation detected here for the Nubian plate is sufficiently small so that a rigid reference frame can safely be attached to Nubia for practical applications.

[56] A static frame may not hold for territories located on the neighboring Somalia, Victoria, or Rovuma plates, where horizontal velocities with respect to Nubia (hence to the core of the frame) are significant (Figure 14). For instance, velocities in half of Ethiopia, Somalia, most of Kenya, and part of Tanzania range from 4 to 5 mm/yr with respect to Nubia. This implies that it would only take 5 years in those regions for a static frame tied to Nubia to deform to a level that would be detectable by precise surveying measurements (assuming again a horizontal precision of 2 cm). It means

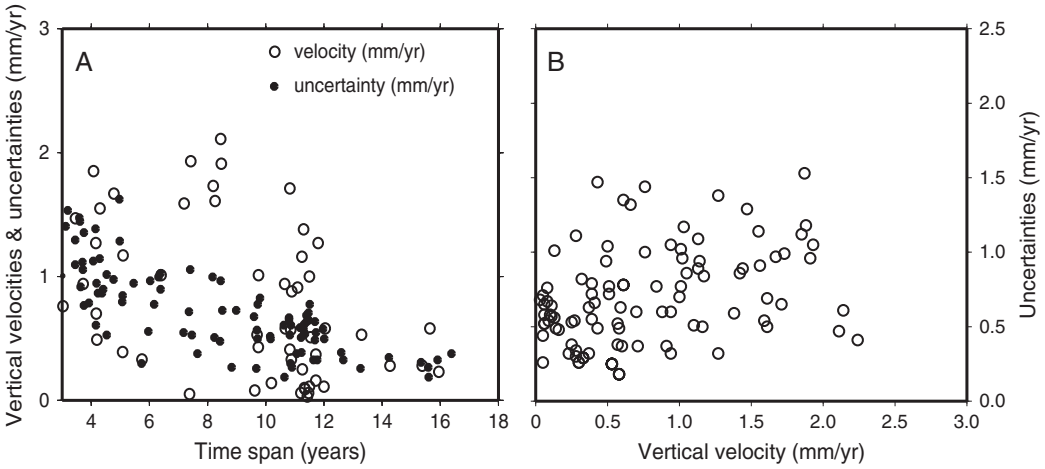


**Figure 20.** (A) Vertical velocities (open circles) and their uncertainties (black circles) as a function of measurement time span. (B) Vertical velocities as a function of the corresponding uncertainty.

that AFREF will likely need to consider being at least partly dynamic in order to avoid distortions that will rapidly accumulate with time across the East African Rift. A similar reasoning may apply to northern Africa, but we do not have sufficient data in this study to quantify the impact of plate boundary deformation in that region on the frame definition.

[57] A possible way of dealing with a deforming territory is to define a dynamic or semidynamic datum [*Tregoning and Jackson*, 1999]. It may be difficult for many users to use a fully dynamic datum, i.e., to include station velocities in their network adjustment. A semidynamic datum provides a useful alternative where network adjustments are computed using positions only, but that are back-propagated to a given origin epoch using a tectonic model. This later approach is used for instance in New Zealand [*Blick et al.*, 2005] and in Papua-New Guinea (Stanaway, R., C. Roberts, and G. Blick (in press), Realisation of a geodetic datum using a gridded absolute deformation model (ADM), *IUGG General Assembly, Melbourne, Australia*). It allows the surveying and mapping community to deal with static coordinates but still accounts for tectonic motions that, if uncorrected, would affect the accuracy of the positioning results. The plate kinematic model provided here for eastern Africa (Figure 17) could be used to define the velocity of any site with respect to the Nubian "core" of the frame.

[58] AFREF stipulates that the frame must be aligned with ITRF. The solution described above shows no significant bias with respect to ITRF2008. In addition, the Nubia-ITRF angular velocity found here is similar to the ITRF2008 estimates (Table 1 and Figure 13). The best way to ensure consistency with ITRF is probably to make sure that the final AFREF solution includes, as its backbone, the full ITRF solution (i.e., full ITRF SINEX file). The velocities of stations defining AFREF will need to be closely monitored in order to ensure consistency over time.

## 6. Conclusion

[59] We derived a new geodetic velocity field for Africa and its surroundings by rigorously combining data from more than 123 continuous GPS sites and nine DORIS sites covering the past 17 years. Velocities on stable Nubia fit a single rigid plate model with a WRMS of 0.6 mm/yr (maximum residual 1 mm/yr), consistent with the current uncertainty of geodetic measurements in the region. This represents an upper bound for plate-wide motions and for regional-scale deformation in active areas such as the seismically active southern Africa and Cameroon volcanic line. However, the current distribution of geodetic sites in Africa is still very uneven, and internal deformation at the regional or local scales may not be detectable with the current networks. We updated the angular velocity describing the divergence between the Nubian and Somalian plates and found a geodetic (present-day) estimate that matches the geologic (3.16 My) one [*DeMets et al.*, 2010]. We determined, using geodetic data alone, the angular velocity describing the current motion of Victoria and Rovuma, two plates embedded within the EAR [*Stamps et al.*, 2008]. Rovuma rotates in a clockwise direction with respect to Nubia, consistent with the clockwise motion of the surrounding Somalia plate. The counterclockwise rotation of Victoria, consistent with previous results, is less intuitive in that context and may require the small-scale effect of mantle processes [e.g., *Calais et al.*, 2006b].

[60] This study provides a continent-wide position/velocity solution for Africa rigorously expressed in ITRF2008 and is therefore an initial contribution to the upcoming African Reference Frame (AFREF). We argue that using a static frame for territories located on stable Nubia is acceptable because of its low level of internal deformation. However, we also argue that deforming territories in northern and eastern Africa should consider using a semidynamic (or preferably dynamic) datum in order to avoid network distortions that would be easily detected given the deformation rates involved and the level of precision currently achievable by well-equipped surveyors. The kinematic model proposed here for East Africa can serve to define such a datum.

[61] In spite of recent progress on GNSS site distribution and open data access in Africa, most of the continent remains largely undersampled. Efforts are underway to augment the geodetic infrastructure through projects such as AFREF, through links with academic research projects, or at national levels for surveying applications. It is important

that these new data sets contribute openly to defining a common reference frame for Africa, an objective that will benefit everyone.

[62] **Acknowledgments.** We acknowledge and thank organizations that make their data openly available to research, with no strings attached. This includes AFREF, the Regional Centre for Mapping of Resources for Development (RCMRD, via AFREF), the Ethiopian Mapping Agency (via AFREF), TRIGNET in South Africa, the Nigerian GNSS Reference Network (NIGNET), AfricaArray (via UNAVCO). We also thank other agencies and individual investigators who contribute their data through these archives or through the IGS data centers, the UNAVCO archive, or other similarly open archives. We thank Oliver Bock for sharing the AMMA data ahead of publication. We acknowledge using the SEGAL archive, which makes a subset of their data available online. We thank the IGS and its contributors for the data and products it provides to the community. This work benefited from discussions with Richard Wonnacott and Robert W. King, with additional input from Robert Reilinger and Mike Floyd. We thank Don Argus and an anonymous reviewer for their constructive comments which significantly contributed to strengthening the paper. This work uses data services provided by the UNAVCO Facility with support from the National Science Foundation (NSF) and National Aeronautics and Space Administration (NASA) under NSF Cooperative Agreement EAR-0735156. ES and EC were supported by NSF award EAR-0538119 to EC. Part of this work was supported by the Centre National d'Etudes Spatiales (CNES) and uses observations from the DORIS instruments on board SPOTs, TOPEX/Poseidon, Envisat, Jason-2, and Cryosat-2 satellites. This paper is IPGP contribution 3373.

## References

Agnew, D. C. (1992), The time-domain behavior of power-law noises, *Geophys. Res. Lett.*, *19*, 333–336.

Al-Hajri, Y., N. White, and S. Fishwick (2009), Scales of transient convective support beneath Africa, *Geology*, *37*(10), 883–886.

Altamimi, Z., P. Sillard, and C. Boucher (2002), ITRF2000: A new release of the international terrestrial reference frame for earth science applications, *J. Geophys. Res.*, *107*(B10), 2214, doi:10.1029/2001JB000561.

Altamimi, Z., X. Collilieux, J. Legrand, B. Garayt, and C. Boucher (2007), ITRF2005: A new release of the international terrestrial reference frame based on time series of station positions and Earth orientation parameters, *J. Geophys. Res.*, *112*, B09401, doi:10.1029/2007JB004949.

Altamimi, Z., X. Collilieux, and L. Métivier (2011), ITRF2008: An improved solution of the international terrestrial reference frame, *J. Geod.*, *85*(8), 457–473, doi:10.1007/s00190-011-0444-4.

Altamimi, Z., L. Métivier, and X. Collilieux (2012), ITRF2008 plate motion model, *J. Geophys. Res.*, *117*, B07402, doi:10.1029/2011JB008930.

Argus, D. F., and R. G. Gordon (1996), Tests of the rigid-plate hypothesis and bounds on intraplate deformation using geodetic data from very long baseline interferometry, *J. Geophys. Res.*, *101*(B6), 13555–13572, doi:10.1029/95JB037.

Argus, D. F., W. R. Peltier, and M. M. Watkins (1999), Glacial isostatic adjustment observed using very long baseline interferometry and satellite laser ranging, *J. Geophys. Res*, *104*, 29077–29083.

Argus, D. F., M. B. Heflin, G. Peltzer, F. Crampè, and F. H. Webb (2005), Interseismic strain accumulation and anthropogenic motion in metropolitan Los Angeles, *J. Geophys. Res.*, *110*(B4), art. B04401., doi:10.1029/2003JB002934.

Argus, D. F., R. G. Gordon, M. B. Heflin, C. Ma, R. Eanes, P. Willis, W. R. Peltier, and S. Owen (2010), The angular velocities of the plates and the velocity of Earth's center from space geodesy, *Geophys. J. Int.*, *180*, 916–960, doi:10.1111/j.1365-246X.2009.04463.X.

Argus, D. F., and W. R. Peltier (2010), Constraining models of postglacial rebound using space geodesy: A detailed assessment of model ICE-5G (VM2) and its relatives, *Geophys. J. Int.*, *181*, 697–723, doi:10.1111/j.1365-246X.2010.04562.X.

Argus, D. F., R. G. Gordon, and C. DeMets (2011), Geologically current motion of 56 plates to the no-net-rotation reference frame, *Geochem. Geophys. Geosyst.*, *12*, Q11001, doi:10.1029/2011GC003751.

Awange, J. L., M. A. Sharifi, W. Keller, and M. Kuhn (2009), GRACE application to the receding Lake Victoria water level and Australian drought, *IAG Symp.*, *133*, 387–396

Begg, G. C., et al. (2009), The lithospheric architecture of Africa: Seismic tomography, mantle petrology and tectonic evolution, *Geosphere*, *5*, 23–50.

Behn, M. A., C. P. Conrad, and P. Silver (2004), Detection of upper mantle flow associated with the African superplume, *Earth Planet. Sci. Lett.*, *224*, 259–274.

Blewitt, G., and D. Lavallée (2002), Effect of annual signals on geodetic velocity, *J. Geophys. Res.*, *107*(B7), 2145, doi:10.1029/2001JB000570.

Blick, G., C. Crook, D. Grant, and J. Beavan (2005), Implementation of a semi-dynamic datum for New Zealand, *IAG Symp.*, *128*, 38–43.

Bock, O., P. Willis, M. Lacarra, and P. Bosser (2010), An intercomparison of DORIS tropospheric delays estimated from DORIS and GPS data, *Adv. Space Res.*, *46*(12), 1648–1660, doi:10.1016/j.asr.2010.05.018.

Bock, Y., R. M. Nikolaidis, and M. Bevis (2000), Instantaneous geodetic positioning at medium distances with the global positioning system, *J. Geophys. Res.*, *105*(B12), 28,223–28,253.

Bock, O., et al. (2008), The West African Monsoon observed with ground-based GPS receivers during AMMA, *J. Geophys. Res.*, *113*, D21105, doi:10.1029/2008JD010327.

Boehm, J., A. Niell, P. Tregoning, and H. Schuh (2006), Global mapping function (GMF), a new empirical mapping function based on numerical weather model data, *Geophys. Res. Lett.*, *33*, L07304, doi:10.1029/2005GL025546.

Bruyninx, C., H. habrich, W. Söhne, A. Kenyeres, G Stangl, and C. Völksen (2012), Enhancement of the EUREF permanent network services and products, *IAG Symp.*, *136*, 27–34.

Calais, E. (1999), Continuous GPS measurements across the western Alps, 1996–1998, *Geophys. J. Int.*, *38*, 221–230.

Calais, E., J. Y. Han, C. DeMets, and J. M. Nocquet (2006a), Deformation of the North American plate interior from a decade of continuous GPS measurements, *J. Geophys. Res.*, *111*, B06402, doi:10.1029/2005JB004253.

Calais, E., C. J. Ebinger, C. Hartnady, and J. M. Nocquet (2006b), Kinematics of the East African rift from GPS and earthquake slip vector data, in *The Afar Volcanic Province Within the East African Rift System*, edited by G. Yirgu, C. J. Ebinger, and P. K. H. Maguire, pp. 9–22, vol. 259, Geol. Soc. Spec. Publ.

Chesley, J. T., R. L. Rudnick, and C. T. Lee (1999), Re-Os systematics of mantle xenoliths from the East African rift: Age, structure, and history of the Tanzanian craton, *Geochim. Cosmochim. Acta*, *63*, 1203–127.

Cilliers, P. J., D. Gouws, B. Opperman, R. T. Wonnacott, and W. L. Combrinck (2003), The South African network of dual-frequency global positioning system satellite receiver base stations: A national asset with many applications and research opportunities, *S. Afr. J. Sci.*, *99*, 51–55.

Craymer, M. R., and M. Piraszewski (2001), The North American reference frame (NAREF): An initiative to densify the ITRF in North America, *Proceedings of KIS 2001: International Symposium on Kinematic Systems in Geodesy, Geomatics and Navigation, June 5–8, 2001,* Banff, Canada, revised July 13, 2001

De Wit, M. J. (2003), Madagascar: Heads it's a continent, tails it's an island, *Annu. Rev. Earth Planet. Sci.*, *31*, 213–248.

Delvaux, D., and A. Barth (2009), African stress pattern from formal inversion of focal mechanism data, *Tectonophysics*, *482*, 105–128, doi:10.1016/j.tecto.2009.05.009.

DeMets, C., R. G. Gordon, and D. F. Argus (2010), Geologically current plate motions, *Geophys. J. Int.*, *181*, 1–80, doi: 10.1111/j.1365-246X.2009.04491.X.

Dixon, T. H., A. Mao, and S. Stein (1996), How rigid is the stable interior of the North American Plate? *Geophys. Res. Lett.*, *23*, 3035–3038

Doucouré, C. M., and M. J. De Wit (2003), Old inherited origin for the present near-bimodal topography of Africa, *J. Afr. Earth Sci.*, *36*, 371–388.

Dow, J., R. E. Neilan, and C. Rizos (2009), The International GNSS Service in a changing landscape of global navigation satellite systems, *J. of Geodesy.*, *83*, 191–198.

Fadil, A., P. Vernant, S. McClusky, R. Reilinger, F. Gomez, D. B. Sari, T. Mourabit, K. Feigl, and M. Barazangi (2006), Active tectonics of the western Mediterranean: Geodetic evidence for roll back of a delaminated subcontinental lithospheric slab beneath the Rif Mountains, Morocco, *Geology*, *34*, 529–532.

Gobinddass, M. L., P. Willis, M. Diament, and M. Menvielle (2010), Refining DORIS atmospheric drag estimation in preparation of ITRF2008, *Adv. Space Res.*, *46* (12), 1566–1577, doi: 10.1016/j.347asr.2010.04.004.

Gobinddass, M. L., P. Willis, A. de Viron, A. Sibthorpe, N. P. Zelensky, J. C. Ries, R Ferland, Y. Bar-Sever, and M. Diament (2009a), Systematic biases in DORIS-derived geocenter time series related to solar radiation pressure mismodeling, *J. Geod.*, *83*(9), 849–858.

Gobinddass, M. L., P Willis, O. de Viron, A. Sibthorpe, N. P. Zelensky, J. C. Ries, R Ferland, Y. Bar-Sever, M. Diament, and F. G Lemoine (2009b), Improving geocenter time series using an empirical rescaling of solar radiation pressure models, *Ad. Space Res.*, *44*(11), 1279–1287.

Gomez, F., W. Beauchamp, and M. Barazangi (2000), Role of the Atlas Mountains (northwest Africa) within the African–Eurasian plate boundary zone, *Geology*, *28*, 775–778.

Gurnis, M., J. Mitrovica, J. Ritsema, and H. J. van Heist (2000), Constraining mantle density structure using geological evidence of surface uplift rates: The case of the African superplume, *Geochem. Geophy. Geosyst.*, *1*, 1020, doi:10.1029/1999GC000035.

Hartnady, C. J. H. (2002), Earthquake hazard in Africa: Perspectives on the Nubia-Somalia boundary, *S. Afr. J. Sci.*, *98*, 425–428.

Herring, T. A. (2003), MATLAB Tools for viewing GPS velocities and time series, *GPS Solutions*, *7*, 194–199, doi:10.1007/s10291-003-0068-0.

Herring, T. A., R. W. King, and S. C. McClusky (2010), Documentation for the GAMIT GPS software analysis, release 10.05, Mass. Inst. of Technol. Cambridge.

Holmes, A. (1945), *Principles of Physical Geology*, 1st ed.Thomas Nelson and Sons, Edinburgh, Scotland.

Horner-Johnson, B. C., R. G. Gordon, and D. F. Argus (2007), Plate kinematic evidence for the existence of a distinct plate between the Nubia and Somalian plates along the Southwest Indian Ridge, *J. Geophys. Res.*, *112*, B05418, doi:10.1029/2006JB004519.

Johnson, H, and D C Agnew (1995), Monument motion and measurements of crustal velocities, *Geophys. Res. Lett.*, *22*, 2905–2908.

Kinabo, B. D., E. A. Atekwana, J. P. Hogan, M. P. Modisi, D. D. Wheaton, and A. B. Kampunzu (2007), Early structural evolution of the Okavango Rift Zone, NW Botswana, *J. Afr. Earth Sci.*, *48*, 125–136.

Kogan, M. G., and G. M. Steblov (2008), Current global plate kinematics from GPS (1995–2007) with the plate-consistent reference frame, *J. Geophys. Res.*, *113*, B04416, doi:10.1029/2007JB005353.

Langbein, J., D. Dzurisin, G. Marshall, R. Stein, and J. Rundle (1995), Shallow and peripheral volcanic sources of inflation revealed by modeling two-color geodimeter and leveling data from Long Valley Caldera, California, 1988–1992, *J. Geophys. Res.*, *100*, 12,487–12,495.

Langbein, J., and H. Johnson (1997), Correlated errors in geodetic time series: Implications for time-dependent deformation, *J. Geophys. Res.*, *102*, 591–603.

Larson, K. M., and D. C. Agnew (1991), Application of the global positioning system to crustal deformation measurement, 1. Precision and accuracy, *J. Geophys. Res.*, *96*(B10), 16,547-16,565.

Le Bail, K. (2006), Estimating the noise in space-geodetic positioning, the case of DORIS, *J. Geod.*, *80*(8–11), 541–565.

Le Gall, B., P. Nonnotte, J. Rolet, M. Benoit, H. Guillou, M. Mousseau-Nonnette, J. Albaric, and J. Deverchére (2007), Rift propagation at craton margin. Distribution of faulting and volcanism in the North Tanzanian Divergence (East Africa) during Neogene times, *Tectonophysics*, *448*, 1–19.

Lithgow-Bertelloni, C., and P. G. Silveri (1998), Dynamic topography, plate driving forces and the Africa superswell, *Nature*, *395*, 269–272.

Lyard, F., F. Lefevre, and T. Letellier (2006), Modelling the global ocean tides: Modern insights from FES2004, *Ocean Dyn.*, *56*(5–6), 394–415, doi:10.1007/s10236-006-0086-x.

Mahsas, A., K. Lammali, K. Yelles, E. Calais, A. M. Freed, and P. Briole (2008), Shallow afterslip following the 2003 May 21, Mw = 6.9 Boumerdes earthquake, Algeria, *Geophys. J. Int.*, *172*(1), 155–166, doi:10.1111/j.1365-246X.2007.03594.x.

Mantovani, E., M. Viti, D. Babbucci, and D. Albarello (2007), Nubia-Eurasia kinematics: An alternative interpretation from Mediterranean and North Atlantic evidence, *Ann. Geophys.*, *50*, 341–366.

Mao, A. L., C. G. A. Harrison, and T. H. Dixon (1999), Noise in GPS coordinate time series, *J. Geophys. Res.*, *104*, 2797–2816.

McCarthy, D. D., and G. Petit (2003), IERS Technical Note 32, Frankfurt am Main: Verlag des Bundesamts fŁur Kartographie und GeodŁasie, *Geophys. J. Int.*, *127*, doi:10.1046/j.1365-246X.2003.02023.

McClusky, S., R. Reilinger, S. Mahmoud, S. Ben D., and A. Tealeb (2003), GPS constraints on Africa (Nubia) and Arabia plate motions, *Geophys. J. Int.*, *155*, 126–138, doi:10.1046/j.1365-246X.2003.02023.

Meghraoui, M., A. Cisternas, and H. Philip (1986), Seismotectonics of the lower Cheliff basin - Structural background of the El-Asnam (Algeria) earthquake, *Tectonics*, *5*, 809–836.

Moreau, C., J.-M. Regnoult, B. Déruelle, and B. Robineau (1987), A new tectonic model for the Cameroon line, central Africa, *Tectonophysics*, *141*, 317–334.

Moucha, R., and A. M. Forte (2011), Changes in African topography driven by mantle convection, *Nat. Geosci.*, *4*, 707–712, doi:10.1038/NGEO1235.

Nahmani, S., O. Bock, and M. N. Bouin (2012), Hydrological deformation induced by the West African Monsoon: Comparison of GPS, GRACE and loading models, *J. Geophys. Res.*, *117*, B05409, doi:10.1029/2011JB009102.

Njome, M. S., S. Manga, and C. E. Suh (2010), Volcanic risk perception in rural communities along the slopes of Mount Cameroon, West-Central Africa, *J. Afr. Earth Sci.*, *58*(4), 608–622, doi:10.1016/j.jafrearsci.2010.08.007.

Nocquet, J.-M., E. Calais, Z. Altamimi, P. Sillard, and C. Boucher (2001), Intraplate deformation in western Europe deduced from an analysis of the ITRF97 velocity field, *J. Geophys. Res.*, *106*, 11,239–11,257.

Nocquet, J. M., and E. Calais (2003), The crustal velocity field in Western Europe from permanent GPS array solutions, 1996–2001, *Geophys. J. Int.*, *154*, 72–88.

Nocquet, J.-M., E. Calais, and B. E. Parsons (2005), Geodetic constraints on glacial isostatic adjustment in Europe, *Geophys. Res. Lett.*, *32*, L06308, doi:10.1029/2004GL022174.

Nocquet, J. M., P. Willis, and S. Garcia (2006), Plate kinematics of Nubia-Somalia using a combined DORIS and GPS solution, *J. Geod.*, *80*, 591–607

Nyblade, A., and S. Robinson (1994), The African superwell, *Geophys. Res. Lett.*, *21*, 765–768.

Nyblade, A. A., T. J. Owens, H. Gurrola, J. Ritsema, and C. A. Langston (2000), Seismic evidence for a deep upper mantle thermal anomaly beneath East Africa, *Geology*, *7*, 599–602.

Pérez-Gussinyé, M., C. J. Swain, J. F. Kirby, and A. R. Lowry (2009), Spatial variations of the effective elastic thickness, Te, using multitaper spectral estimation and wavelet methods; Examples from synthetic data and application to South America, *Geochem, Geophys. Geosyst.*, *10*, doi:10.1029/2008GC002229.

Prawirodirdjo, L., and Y. Bock (2004), Instantaneous global plate motion model from 12 years of continuous GPS observations, *J. Geophys. Res.*, *109*, B08405, doi:10.1029/2003JB002944.

Quéré, S., and A. M. Forte (2006), Influence of past and present-day plate motions on spherical models of mantle convection: Implications for mantle plumes and hotspots, *Geophys. J. Int.*, *165*, 1041–1057.

Reilinger, R., et al. (2006), GPS constraints on continental deformation in the Africa-Arabia-Eurasia continental collision zone and implications for the dynamics of plate interactions, *J. Geophys. Res.*, *111*, B05411, doi:10.1029/2005JB004051.

Ritsema, J., H. J. van Heijst, and J. H. Woodhouse (1999), Complex shear wave velocity structure imaged beneath Africa and Iceland, *Science*, *286*, 1925–1928, doi:10.1126/science.286.5446.1925.

Sanchez, L., W. Seemueller, and M. Seitz (2012), Combination of the weekly solutions delivered by the SIRGAS Processing centres for the SIRGAS-CON reference frame, *IAG Symp.*, *136*, 845–851, doi:10.1007/978-3-642-20338-1_106.

Schmid, R., P. Steigenberger, G. Gendt, M. Ge, and M. Rothacher (2007), Generation of a consistent absolute phase-center correction model for GPS receiver and satellite antennas, *J. Geod.*, *81*, 781–798, doi:10.1007/s00190-007-0148-y.

Sebagenzi, M. N., and K. Kaputo (2002), Geophysical evidences of continental break up in the southeast of the Democratic Republic of Congo and Zambia (Central Africa), in *From Continental Extension to Collision: Africa-Europe Interaction, the Dead Sea and Analogue Natural Laboratories,* vol. 2, edited by S. A. P. L. Cloetingh, and Z. Ben-Avraham, pp. 193-206, Stephan Mueller Special Publication Series, EGU European Geosciences Union.

Sella, G. F., T. H. Dixon, and A. Mao (2002), REVEL : A model for recent plate velocities from space geodesy, *J. Geophys. Res.*, *107*, 2081, doi:10.1029/2000JB00033.

Sella, G. F., S. Stein, T. H. Dixon, M. Craymer, T. S. James, S. Mazzotti, and R. K. Dokka (2007), Observation of glacial isostatic adjustment in "stable" North America with GPS, *Geophys. Res. Letters*, *34*(2), L02306, doi:10.1029/2006GL027081.

Stamps, D. S., E. Calais, E. Saria, C. Hartnady, J. M. Nocquet, C. Ebinger, and R. Fernandez (2008), A kinematic model for the East African Rift, *Geophys. Res. Letters*, *35*, L05304, doi:10.1029/2007GL032781.

Stein, S., and R. G. Gordon (1984), Statistical tests of additional plate boundaries from plate motion inversions, *Earth planet. Sci. Lett.*, *69*, 401–412.

Švábenský, O., and J. Weigel (2004), Optimized technology for GPS height determination FIG working week, Athens, Greece, May 22–27, 2004.

Tavernier, G., et al. (2002), Current status of the DORIS pilot experiment and the future international DORIS service, *Adv. Space Res.*, *30*(2), 151–156.

Tedesco, D., O. Vaselli, P. Papale, S. A. Carn, M. Voltaggio, G. M. Sawyer, J. Durieux, M. Kasereka, and F. Tassi (2007), January 2002 volcano-tectonic eruption of Nyiragongo volcano, Democratic Republic of Congo, *J. Geophys. Res.*, *112*, B09202, doi:10.1029/2006JB00-4762.

Tregoning, P., and R. Jackson (1999), The need for dynamic datums, *Geomatics Research Australasia*, *71*, 87–102.

Tregoning, P. (2003), Is the Australian Plate deforming? A space geodetic perspective, *Geol. Soc. Aus Spec. Pub.*, *37*, 41–48

Tokam, K. A. P. (2010), Crustal structure beneath Cameroon (West Africa) deduced from the joint inversion of Rayleigh wave group velocities and receiver functions, PhD thesis, University of Yaounde.

Ubangoh, R. U., B. Ateba, S. N. Ayonghe, and G. E. Ekodeck (1997), Earthquake swarms of Mt Cameroon, west Africa, *J. Afr. Earth Sci.*, *24*(4), 413–424.

vanDam, T., J. Wahr, P. M. Milly, A. Shmakin, G. Blewitt, D. Lavallée, and K. Larson (2001), Crustal displacements due to continental water loading, *Geophys. Res. Letters*, *28*, 651–654.

Vicat, J. P., A. Pouclet, Y. Bellion, and J. C. Doumnang (2002), The peralkaline rhyolites (pantellerites) of the Lake Chad. Composition and tectonomagmatic significance, *C.R. Geosci.*, *334*, 885–891.

Webb, F., and J. Zumberge, (1995), An introduction to GIPSY-OASIS-II, *Tech. Rep. JPL D-11088*, Calif. Inst Tech., Pasadena, CA.

Weeraratne, D. S., D. W. Forsyth, K. M. Fischer, and A. A. Nyblade (2003), Evidence for an upper mantle plume beneath the Tanzanian craton from Rayleigh wave tomography, *J. Geophys. Res.*, *108*(B9), 2427, doi: 10.1029/2002JB002273.

Williams, S. D. P. (2003), The effect of coloured noise on the uncertainties of rates estimated from geodetic time series, *J. Geod.*, *76*, 483–494, doi: 10.1007/s00190-002-0283-4.

Williams, S. D. P., Y. Bock, P. Fang, P. Jamason, R. M. Nikolaidis, L. Prawirodirdjo, M. Miller, and D. J. Johnson (2004), Error analysis of continuous GPS time series, *J. Geophys. Res.*, *109*, B03412, doi: 10.1029/2003JB002741.

Williams, S. D. P., and P. Willis (2006), Error analysis of weekly station coordinates in the DORIS network, *J. Geod.*, *80*(8–11), 525–539.

Williams, S. D. P. (2008), CATS: GPS coordinate time series analysis software, *GPS Solut.*, *12*(2), 147–153, doi:10.1007/s10291-007-0086-4.

Willis, P., and J. C. Ries (2005), Defining a DORIS core network for Jason-1 precise orbit determination based on ITRF2000, methods and realization, *J. Geod.*, *79*, 370–378, doi: 10.1007/s00190-005-0475-9.

Willis, P., Y. Bar-Sever, and G. Tavernier (2005a), DORIS as a potential part of a global geodetic observing system, in IGGOS science rationale, H. Drewes (Ed.), *J. Geodyn.*, *40*, 494–501, doi: 10.1016/j.jog.2005.06.011.

Willis, P., C. Boucher, H. Fagard, and Z. Altamimi (2005b), Geodetic applications of the DORIS system at the French "Institut Géographique National", *CR. Geosci.*, *337*, 653–662, doi: 10.1016/j.crte.2005.03.002.

Willis, P., et al. (2010a), The international DORIS service, toward maturity, *Adv. Space Res.*, *45*, 1408–1420.

Willis, P., C. Boucher, H. Fagard, B. Garayt, and M. L. Gobinddass (2010b), Contributions of the French Institut Géographique National (IGN) to the international DORIS service, *Adv. Space Res.*, *45*, 1470–1480, doi:10.1016/j.asr.2009.09.019.

Willis, P., M. L. Gobinddass, B. Garayt, and H. Fagard (2012), Recent improvements in DORIS data processing in view of ITRF2008, the ignwd08 solution, *IAG Symposia Series*, *136*, 43–49, doi: 10.1007/978-3-64.

Wonnacott, R. T. (2005), AFREF: Background and progress towards a unified reference system for Africa, *Proceedings FIG Working Week 2005, 16–21 April 2005, Cairo Egypt*

Wonnacott, R. T., (2006), The AFREF project: A progress report, *AFREF Technical Workshop*, Cape Town, July 2006.

Wyatt, F. (1989), Displacements of surface monuments: Vertical motion, *J. Geophys. Res.*, *94*, 1655–1664.

Zhang, J., Y. Bock, H. Johnson, P. Fang, J. F. Genrich, S. Williams, S. Wdowinski, and J. Behr (1997), Southern California permanent GPS geodetic array: Error analysis of daily position estimates and site velocities, *J. Geophys. Res.*, *102*, 18,035–18,055.